

Beyond single techniques: can a hybrid MCDM approach re-define flood risk mapping and decision-making in Sub-Himalayan North Bengal?

Debarshi Ghosh, Sanjoy Mandal, Dipankar Das, Edris Alam & Snehasish Saha

To cite this article: Debarshi Ghosh, Sanjoy Mandal, Dipankar Das, Edris Alam & Snehasish Saha (2026) Beyond single techniques: can a hybrid MCDM approach re-define flood risk mapping and decision-making in Sub-Himalayan North Bengal?, *Geocarto International*, 41:1, 2630429, DOI: [10.1080/10106049.2026.2630429](https://doi.org/10.1080/10106049.2026.2630429)

To link to this article: <https://doi.org/10.1080/10106049.2026.2630429>



© 2026 The Author(s). Published by Informa UK Limited, trading as Taylor & Francis Group.



Published online: 17 Feb 2026.



Submit your article to this journal



View related articles



CrossMark

View Crossmark data

Beyond single techniques: can a hybrid MCDM approach re-define flood risk mapping and decision-making in Sub-Himalayan North Bengal?

Debarshi Ghosh^a , Sanjoy Mandal^b , Dipankar Das^c , Edris Alam^d  and Snehasish Saha^b

^aDepartment of Geography, Dhupguri Girls' College, Dhupguri, Jalpaiguri, WB, India; ^bDepartment of Geography & Applied Geography, University of North Bengal, Darjeeling, India; ^cCooch Behar Panchanan Barma University, Cooch Behar, WB, India;

^dFaculty of Resilience, Rabdan Academy, Abu Dhabi, United Arab Emirates

ABSTRACT

Flood susceptibility mapping in the Sub-Himalayan piedmont of North Bengal is difficult because flood footprints shift and multiple drivers interact. We propose a transparent GIS-based hybrid MCDM ensemble that integrates TOPSIS, VIKOR, EDAS and PROMETHEE-II after min-max normalization and direction-of-influence harmonization (higher values indicate higher susceptibility). To retain interpretability, the four model outputs are equally weighted, while PROMETHEE-GAIA provides post-hoc insight into factor contributions. Validation using an independent multi-event flood inventory shows improved discrimination and calibration over single methods ($AUC = 0.80$, 95% CI 0.76–0.82; Brier = 0.200; DeLong significant). Five susceptibility classes identify High-Very High hotspots along the Torsa-Raidak-Jaldhaka corridors and low-lying confluences, with >70% of High-Very High cells within ~2 km of major channels. Tufanganj I-II and Mathabhanga I emerge as priority blocks for screening and mitigation. Polar-plot diagnostics complement probability metrics, supporting corridor-focused drainage maintenance in data-limited Himalayan piedmonts.

ARTICLE HISTORY

Received 5 June 2025

Accepted 7 February 2026

KEYWORDS

Flood susceptibility mapping; multi-criteria decision-making; ensemble; PROMETHEE-GAIA; North Bengal; Sub-Himalayan piedmont

1. Introduction

Flooding in the lowlands (Tal region) of Sub-Himalayan North Bengal and the piedmont zones of the Bhutanese Hills is a persistent hazard, exacerbated by intense monsoonal precipitation, steep topography, and hydrological complexities (Ahmad et al. 2019; Rahmati et al. 2020). The region's susceptibility to flash floods, riverbank erosion, and prolonged inundation necessitates a robust Flood Susceptibility Mapping (FSM) framework to aid in mitigation and preparedness (Kazakis et al. 2015; Tehrany et al. 2019). Traditional FSM methods, such as logistic regression, frequency ratio, and statistical models, often fall short in accommodating the multi-dimensionality of flood risk factors, leading to inconsistent and region-specific results (Panahi et al. 2021; Pham et al. 2021). Recent advancements in machine learning and artificial intelligence have improved prediction accuracy, yet their black-box nature and computational complexity limit their practical application in regional flood management (Chapi et al. 2017; Mosavi et al. 2018). Multi-Criteria Decision-Making (MCDM) models such as TOPSIS, VIKOR, EDAS, and PROMETHEE-II have increasingly gained recognition in flood risk studies. These approaches provide a structured and transparent framework that allows researchers to evaluate risk by simultaneously considering hydrological, geomorphological, and socio-environmental parameters (Bui et al. 2019; Islam 2025; Khosravi et al. 2020). Despite their effectiveness, most FSM studies rely on standalone MCDM techniques, overlooking the potential of hybridization to integrate their distinct methodological advantages (Yariyan et al. 2020; Avand et al. 2021; Kar et al. 2022). TOPSIS, for instance, determines the optimal flood-prone zones by ranking alternatives based on proximity to an ideal solution, while VIKOR emphasizes compromise solutions, making it particularly useful for resolving uncertainties in flood risk (Ouma and Tateishi 2014; Nguyen and Bae 2019). EDAS refines decision-making by evaluating the deviation of alternatives

CONTACT Dipankar Das  dasdipankar783@gmail.com

© 2026 The Author(s). Published by Informa UK Limited, trading as Taylor & Francis Group.

This is an Open Access article distributed under the terms of the Creative Commons Attribution License (<http://creativecommons.org/licenses/by/4.0/>), which permits unrestricted use, distribution, and reproduction in any medium, provided the original work is properly cited. The terms on which this article has been published allow the posting of the Accepted Manuscript in a repository by the author(s) or with their consent.

from an average solution, ensuring more balanced rankings (Yariyan et al. 2020; Ghorbanzadeh et al. 2020). PROMETHEE-II, with its preference-based ranking system, enables better spatial prioritization of flood vulnerability zones (Kazakis et al. 2015; Abdullah et al. 2021). However, no single model comprehensively captures the complex interactions between flood-conditioning factors, necessitating a rational hybridization of these MCDM techniques to achieve a more accurate and robust FSM framework (Razavi Termeh et al. 2018; Barros et al. 2022; Pourghasemi et al. 2020).

Given the recurrent floods, several studies have attempted to map flood susceptibility in Koch Bihar using GIS and multi-criteria or statistical models. Early approaches often combined hazard indicators (e.g. flood frequency, rainfall intensity, elevation, distance to river) with vulnerability factors (e.g. population, land use, infrastructure) to produce flood risk zonation maps. One notable previous work applied the Analytical Hierarchy Process (AHP) with GIS to integrate multiple criteria into a flood risk index for the entire Cooch Behar district (Koch Bihar) (Chakraborty and Mukhopadhyay 2019). Another approach focused on urban flooding in the Cooch Behar (Koch Bihar) urban agglomeration used a GIS-based AHP model to map flash flood susceptibility at city scale. (Choudhury et al. 2022) selected 12 influencing factors (e.g. land use, NDVI, distance to river, road density, drainage, etc.), performed multi-collinearity tests to avoid redundant variables, and then weighted the factors via AHP. In addition to AHP, researchers have explored data-driven statistical models for flood susceptibility in the region. For example, frequency ratio (FR), weight-of-evidence (WoE), and logistic regression (LR) models have been tested to predict flood-prone areas using past flood occurrence points and terrain characteristics. More recently, multi-criteria decision-making (MCDM) techniques beyond AHP have been applied in Koch Bihar to improve flood susceptibility mapping. In another work, we observed the use of three standalone MCDM methods viz. TOPSIS, VIKOR and EDAS for flood susceptibility in Koch Bihar (often spelled *Koch Bihar* in their work) (Mitra et al. 2022). The fact that their results, while broadly similar, were not identical implies some uncertainty when relying on a single technique. For instance, differences between VIKOR and EDAS outputs could lead to different interpretations of which specific locations are most at risk. This raises a challenge like which map does a decision-maker trust if different models yield slightly different hotspot zones? Past studies in Koch Bihar up to this point have not fully resolved this, as they generally applied one method at a time (or compared methods separately). Single-technique models may either lack integration as unable to leverage the complementary strengths of other approaches or lack interpretability for end-users. At the global scale, most comparable works have similarly applied standalone MCDM methods, including TOPSIS in Greece (Kazakis et al. 2015), VIKOR in Iran (Khosravi et al. 2018), EDAS in Turkey (Yariyan et al. 2020) or PROMETHEE-II in coastal Europe (Barros et al. 2022). Such models have demonstrated local success but often produced results with limited transferability, methodological transparency, or interpretability for policymakers. Addressing the features and drawbacks of standalone models, we are proposing a rational hybridization of the four MCDM approaches, augmented with the PROMETHEE-GAIA decision-support tool to enhance both predictive performance and interpretability for decision-makers.

By combining models, the ensemble model may achieve higher validation performance than any individual method alone. A critical research gap lies in the lack of an integrated FSM model that systematically combines the strengths of multiple MCDM techniques while minimizing their individual weaknesses (Acharya and Joshi 2020; Ghobadi and Ahmadipari 2024; Ghorbani et al. 2021). Previous studies have primarily applied TOPSIS, VIKOR, EDAS, or PROMETHEE-II in isolation, limiting their predictive capacity (Paul et al. 2019; Zhao et al. 2021). Moreover, existing flood susceptibility models often fail to incorporate decision-support tools that enhance interpretability and real-world applicability (Khosravi et al. 2018; Maqsoom et al. 2021). This study bridges these gaps by proposing the first rational hybridization of TOPSIS, VIKOR, EDAS and PROMETHEE-II, supported by the PROMETHEE-GAIA (Geometrical Analysis for Interactive Aid) method (de Brito et al. 2019; Bui et al. 2020). PROMETHEE-GAIA provides a visual representation of alternative rankings, facilitating better decision-making for policymakers and disaster management authorities (Shams et al. 2024; Behzadian et al. 2010). By integrating GIS-based analytics with hybridized MCDM techniques, this study aims to develop a scientifically robust FSM framework tailored to the unique hydrological and geomorphological conditions of Sub-Himalayan North Bengal. The proposed methodology enhances flood risk assessment by offering a more holistic and adaptive approach, ensuring improved prioritization of flood-prone zones and optimized

resource allocation for flood mitigation. Given the limitations of empirical and deterministic models, there is an urgent need for advanced multi-criteria decision-making (MCDM) approaches to assess and prioritize flood-prone zones with higher accuracy (Arabameri et al. 2018; Pourghasemi et al. 2020; Ouma and Tateishi 2014). Given Cooch Behar's (Koch Bihar) significance as a transboundary flood-affected region along the India-Bangladesh corridor, the findings of this study will contribute to flood susceptibility mapping as a decision-support input to broader flood management and sustainable water management policies. This study therefore aims to develop a GIS-based hybrid flood susceptibility mapping (FSM) framework by integrating four widely used MCDM techniques-TOPSIS, VIKOR, EDAS and PROMETHEE-II supported by the PROMETHEE-GAIA decision-support tool. The specific objectives are: (i) to enhance the accuracy and reliability of flood susceptibility assessment through rational hybridization of MCDM models, (ii) to delineate flood-prone zones in Koch Bihar district under Sub-Himalayan North Bengal conditions and (iii) to compare the performance of the hybrid model against individual MCDM techniques using multiple validation metrics.

2. Study area

Cooch Behar District (Koch Bihar), located in the north-eastern part of West Bengal, India, lies south of the Bhutanese Hills, forming part of the internationally recognized Sub-Himalayan piedmont region. The district spans approximately 3,345 square km and is positioned within the active floodplain of the Torsa, Jaldhaka, Kaljani, Raidak and Sankosh major river systems (Figure 1), which originate in the Eastern Himalayas and are known for their dynamic geomorphological characteristics (Rahmati et al. 2020; Khosravi et al. 2020). Elevations in the district range from 20 to 50 meters above sea level, making it one of the lowest-lying flood-prone zones in this Himalayan foothill landscape (Kazakis et al. 2015; Saha et al. 2023). Administratively, Koch Bihar is divided into several sub-districts (blocks), including Koch Bihar I, Koch Bihar II, Mathabhanga I, Mathabhanga II, Tufanganj I, Tufanganj II, Dinhata I, Dinhata II, Sitalkuchi and Sitai. The district experiences a humid subtropical monsoon climate, with an average annual rainfall exceeding 3,000 mm,

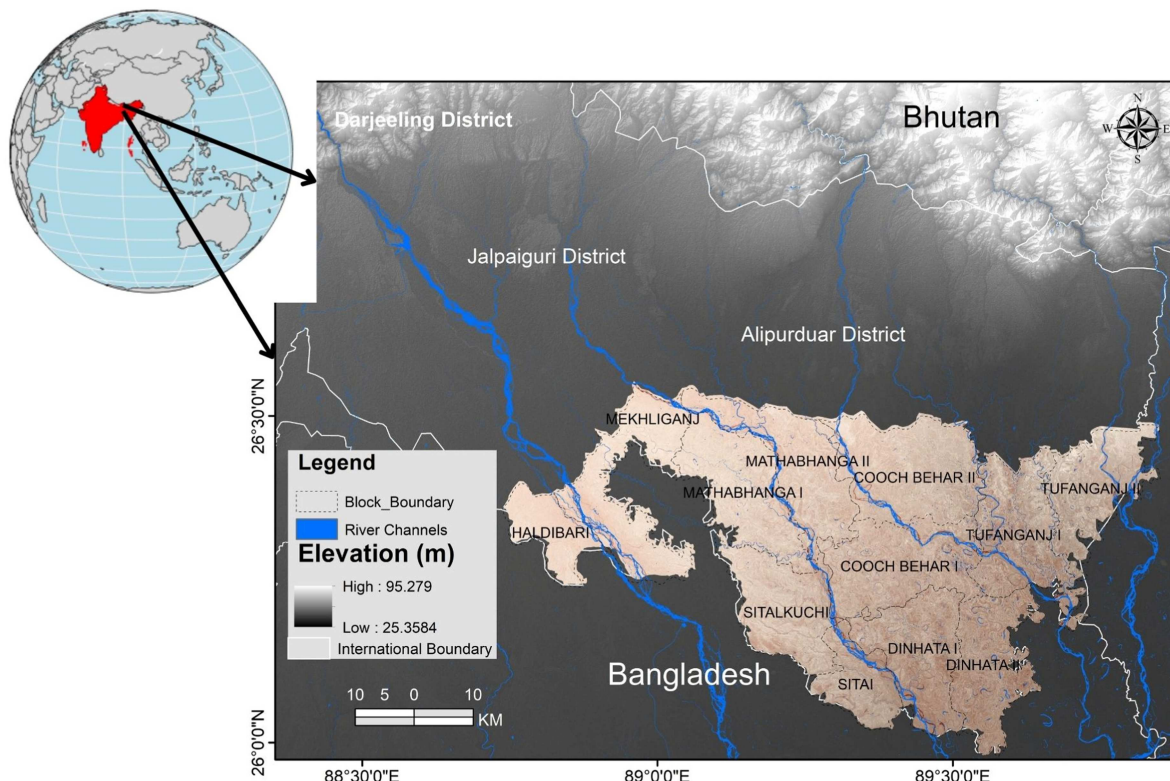


Figure 1. Location map of Sub-Himalayan North Bengal with Cooch Behar (Koch Bihar) district.

which significantly contributes to its recurrent flood susceptibility (Mosavi et al. 2018; Chakraborty and Mukhopadhyay 2019). Koch Bihar has experienced recurrent monsoon floods driven by the Torsa–Kaljani–Raidak–Jaldhaka–Gadadhar River system, with district records noting major flood episodes in 1993, 2006–2010, 2017, 2019, 2020, and 2023, affecting up to ~50% of the district area and ~30–40% of the population in severe years (Ghosh and Ghosal 2021; Roy et al. 2021). During August 2017, excessive rainfall in the Torsa and Raidak catchments (9–14 Aug) triggered widespread inundation; rivers crossed danger levels, portions of NH-31 were submerged near Maruganj, and at least 2.87 lakh people were affected in Koch Bihar with more than 550 relief centres opened (Chakraborty and Mukhopadhyay 2019). In late June 2020, the district recorded 428.5 mm rainfall between 24–29 June against a normal 129.5 mm ($\approx 231\%$ above normal), coinciding with high flood stages of the Torsa and associated damages reported in the state flood bulletins (Khosravi et al. 2020; Rahmati et al. 2020). Recent flood seasons, particularly in 2023, again witnessed multiple heavy-rainfall spells across North Bengal with significant flood impacts in Cooch Behar (Koch Bihar), underscoring its chronic vulnerability to monsoonal flooding (Roy et al. 2021; Ghosh et al. 2022). The interaction between high-intensity monsoonal precipitation and the region's intricate river network results in frequent overbank flooding and waterlogging, exacerbated by river course migration and sediment deposition. Flood susceptibility mapping (FSM) in Koch Bihar is crucial for sustainable disaster management and climate resilience planning. However, past research on FSM in the region has largely relied on conventional GIS-based statistical models and hydrological simulations, which do not effectively integrate multi-dimensional decision-making parameters (Khosravi et al. 2018; Ghorbani et al. 2021).

3. Driver variables

The driver variables (Table 1) employed in this study were meticulously chosen based on their demonstrated relevance to flood susceptibility, data availability, and significant roles highlighted in prior research. The overall methodological framework has been outlined as a workflow diagram from data acquisition to model validation (Figure 2). Total of 20 flood-conditioning factors were integrated into the MCDM-based flood susceptibility mapping framework to provide a comprehensive analysis of flood-prone areas (Tehrany et al. 2019; Abedi Gheshlaghi et al. 2020). All predictors were first harmonized to a common spatial reference and grid before modelling. Specifically, rasters were reprojected to UTM 45N, WGS-84 and co-registered to a single pixel size (30 m for DEM-derived products; 10 m layers upscaled to 30 m), using bilinear resampling for continuous variables (e.g. ARF, SPI, TWI, NDVI, MNDWI) and nearest-neighbour for categorical layers (LCC, STX) to preserve class integrity (Malczewski 1999). To place heterogeneous variables on a comparable footing for MCDM aggregation, we have applied min-max normalization to [0, 1] for all continuous predictors after outlier control. Because some flood drivers act in opposite directions, we performed direction-of-influence harmonization so that larger normalized values always indicate higher flood susceptibility ('benefit-type' for the MCDM). Categorical layers (LCC, STX) were reclassified to [0, 1] via literature-supported susceptibility scores (e.g. higher weights for built-up/bare, lower for forest/agriculture), then checked with sensitivity analysis (Kazakis et al. 2015; Liu et al. 2015). We have screened predictors using Spearman's ρ and variance inflation factor; where $|\rho| \geq 0.70$ or $VIF > 5$, we have retained the variable with stronger theoretical relevance and/or higher permutation importance in preliminary runs (O'Brien 2007). The resulting [0, 1] standardized stack ensures comparability across disparate units (e.g. rainfall vs. NDVI) and supports a dimensionless, weight-integrable MCDM overlay from which the susceptibility index is derived (Abdel Hamid et al. 2020; Demissie et al. 2024). Topographic factors included elevation (ELE) and slope (SLP) (Figure 3a, b), Topographic Ruggedness Index (TRI) (Figure 4i), Geomorphology(GM) (Figure 3g), Topographic Position Index (TPI) (Figure 5p), curvature (CUR) (Figure 5t) and aspect (ASP), all derived from ASTER DEM and Shuttle Radar Topography Mission (SRTM) data. These variables influence water accumulation, runoff velocity and retention capacities, with flatter and lower elevation areas typically showing higher susceptibility (Kazakis et al. 2015; Liu et al. 2015). Hydrological parameters consisted of Drainage Density (DD) (Figure 3c), Stream Power Index (SPI) (Figure 3h), Topographic Wetness Index (TWI) (Figure 4j), and Distance from River (DFR) (Figure 3d). These were computed via GIS-based hydrological modelling to evaluate the role of river networks and watershed dynamics in flood occurrences (Srivastava and Bhattacharya 2006; Kumar and Acharya 2016). Climatic and meteorological variables included Annual Rainfall (ARF) (Figure 3f), rainfall erosivity factor (REF) (Figure 3e), and Modified Fournier Index (MFI) (Figure 5r), collectively accounting for precipitation

Table 1. Data sources.

SL. No	Data type	Description	Source
1	DEM	COP DEM (30 m)	Copernicus Open Access Hub (ESA) https://scihub.copernicus.eu/
2	Soil Texture	Soil Region and sub-order associations of India; RF 1:7,000,000	NBSS and LUP
3	Soil Moisture	SMAP L-band radiometer data, version 1.0 beta (40 km)	MOSDAC (mosdac.gov.in)
4	Land cover	Sentinel 2 A	Copernicus Open Access Hub (ESA), Sentinel-2A data. https://scihub.copernicus.eu/
5	Rainfall	Monthly rainfall	IMD Pune (imdpune.gov.in)
6	Distance From River	Derived from DEM	
7	Geomorphology	RF 1:50000	Bhukosh (gsi.gov.in)
8	Rainfall Erosivity	Global Rainfall Erosivity Data	European Soil Data Centre (ESDAC) - European Commission https://esdac.jrc.ec.europa.eu/content/global-rainfall-erosivity
9	Slope	Derived from DEM	Copernicus Open Access Hub (ESA) https://scihub.copernicus.eu/
10	Drainage Density	Derived from DEM	
11	Stream Power Index	Derived from DEM	
12	Topographic Roughness Index (TRI)	Derived from DEM	
13	Topographic Wetness Index (TWI)	Derived from DEM	
14	NDVI	Normalized Difference Vegetation Index from Sentinel 2 A	Copernicus, Sentinel-2A Bands Used Band 8 (Near Infrared - NIR): 0.842 μ m (10 m resolution) and Band 4 (Red): 0.665 μ m (10 m resolution)
15	SAVI	Soil Adjusted Vegetation Index from Sentinel 2 A	Copernicus, Sentinel-2A Bands Used: Band 8 (Near Infrared - NIR): 0.842 μ m (10 m resolution) & Band 4 (Red): 0.665 μ m (10 m resolution), L Factor: Typically, L = 0.5 is used as a soil brightness correction factor for areas with intermediate vegetation cover.
16	Land Cover Classification	ESRI Global Land Cover Map (10m), 2020.	https://livingatlas.arcgis.com/landcover/
17	Topographic Position Index (TPI)	Derived from DEM	
18	MNDWI	Modified Normalized Difference Water Index from Sentinel 2 A	Sentinel-2A Bands Used: Band 3 (Green): 0.560 μ m (10 m resolution), Band 11 (Shortwave Infrared - SWIR): 1.610 μ m (20 m resolution)
19	Moisture Factor Index (MFI)	Derived from rainfall data	IMD Pune (imdpune.gov.in)
20	Relative Density (RD)	Derived from DEM	
21	Curvature	Terrain Curvature (Concave, Flat, Convex) derived from DEM	
22	Global river flood hazard maps	The global river flood hazard maps are a gridded data set representing inundation along the river network, for seven different flood return periods	European Commission, Joint Research Centre (JRC)
23	2017 Flood Inundation	The Sentinel-1 mission provides data from a dual-polarization C-band Synthetic Aperture Radar (SAR) instrument at 5.405 GHz (C band)	Copernicus Sentinel Data

intensity and its erosional impact as primary triggers for flooding (Pai et al. 2014; Lyu et al. 2016). Vegetation and land-surface factors incorporated into the model were Normalized Difference Vegetation Index (NDVI) (Figure 4k), Soil Adjusted Vegetation Index (SAVI) (Figure 4l), Relative Density (RD) (Figure 5s), Modified Normalized Difference Water Index (MNDWI) (Figure 5q), and land cover classification (LCC) (Figure 5o), extracted from Sentinel-2A imagery. These indices characterize how vegetation cover and surface water features influence infiltration and surface runoff processes (Duchemin and Hogue 2009; Zhao et al. 2021). Soil characteristics, specifically Soil Texture (STX) (Figure 4m) and Soil Moisture (SM) (Figure 4n), were obtained from the National Bureau of Soil Survey & Land Use Planning (NBSS-LUP) and SMAP L-band radiometer data. Their permeability and water retention capacities are crucial for determining how long floodwaters persist in a given area (Bannari et al. 2017). Collectively, these geo-environmental variables enabled a robust, comprehensive, and data-driven assessment essential for effective flood susceptibility mapping using the MCDM approach (Pourghasemi et al. 2020; Rahmati et al. 2020).

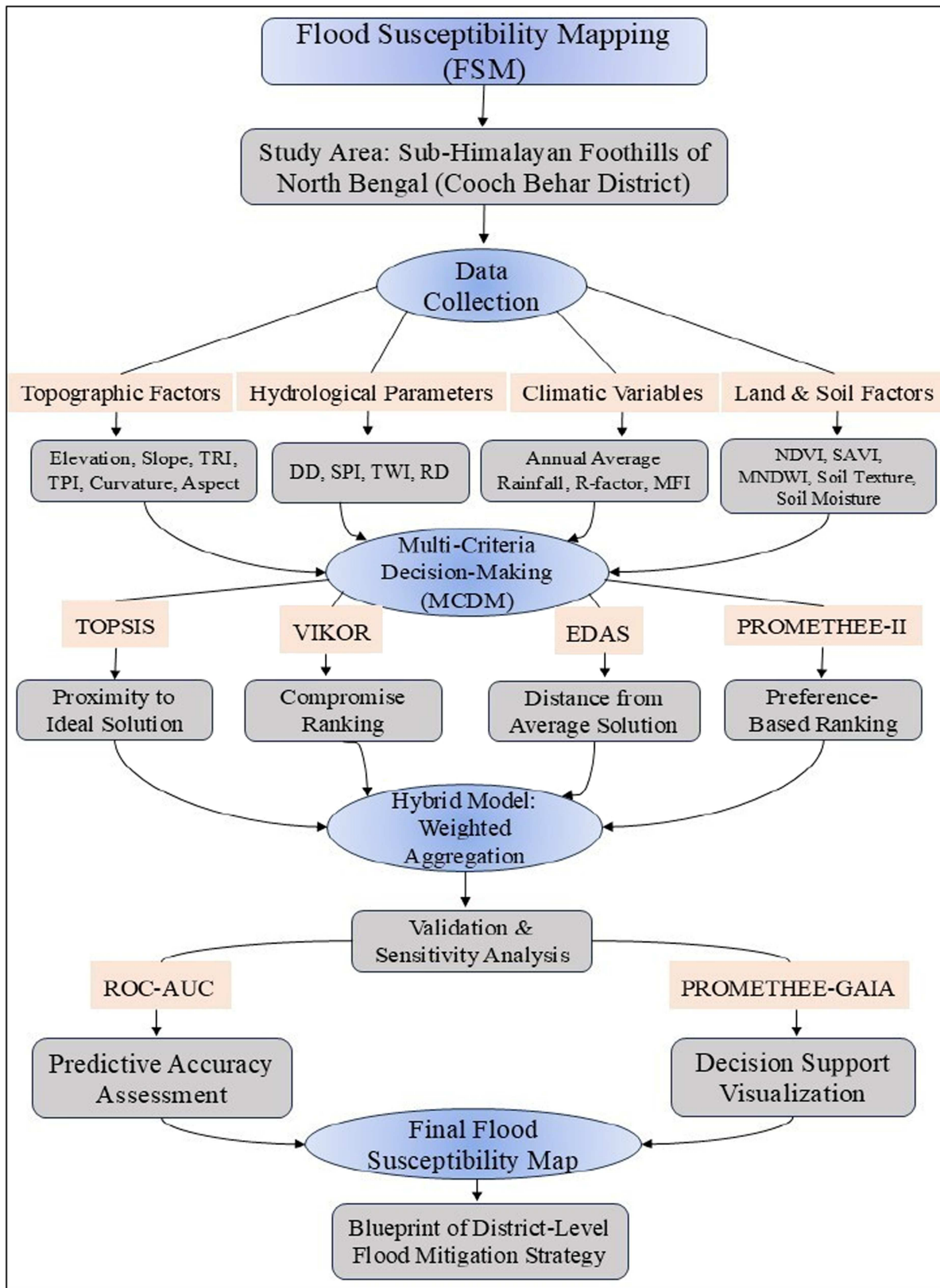


Figure 2. Methodological flow diagram of the study.

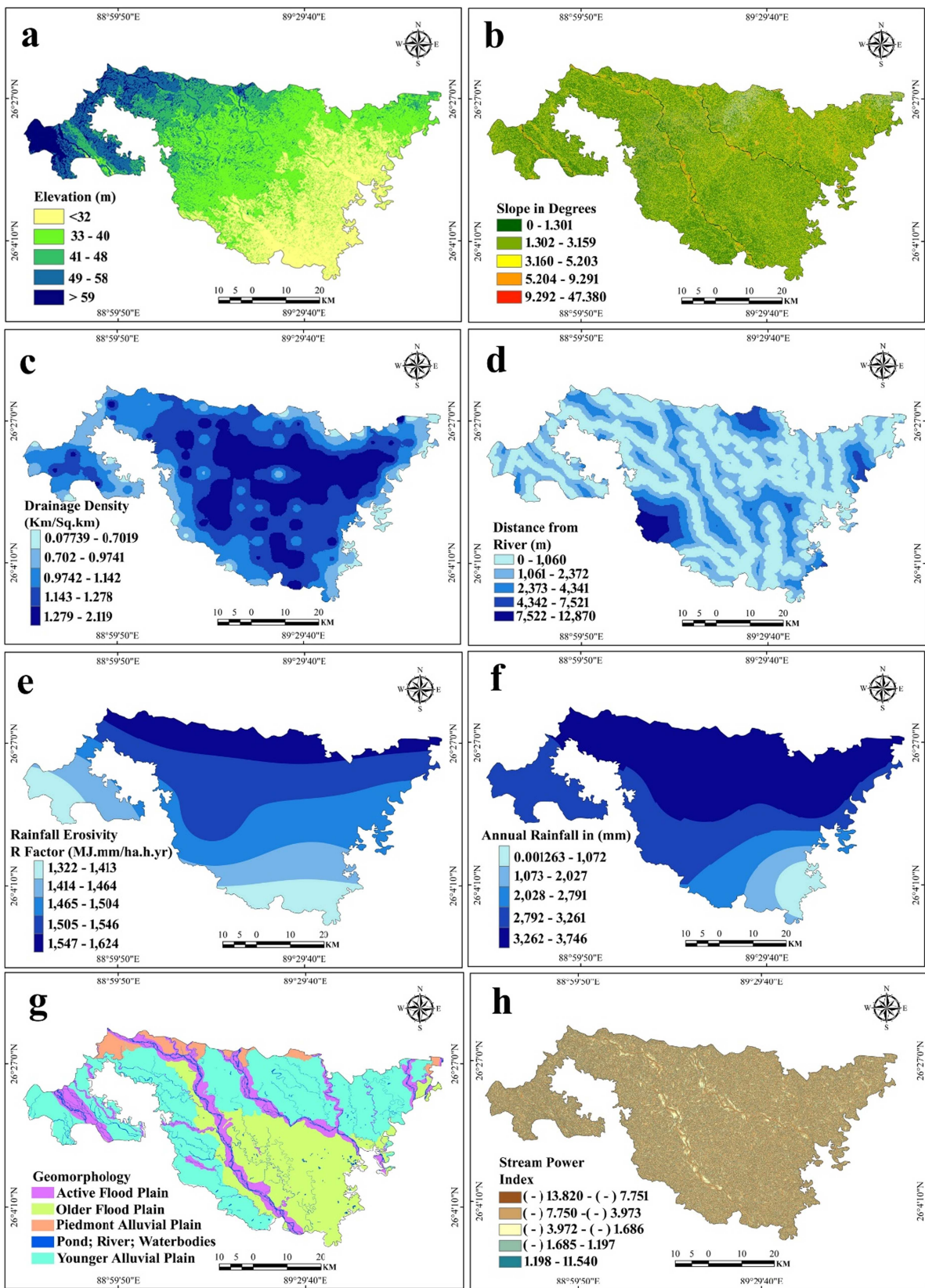


Figure 3. Driver variables: (a) elevation (m), (b) slope (degree), (c) drainage density (km/km^2), (d) distance from river (m), (e) rainfall erosivity factor (R factor), (f) annual rainfall (mm), (g) geomorphology, (h) stream power index.

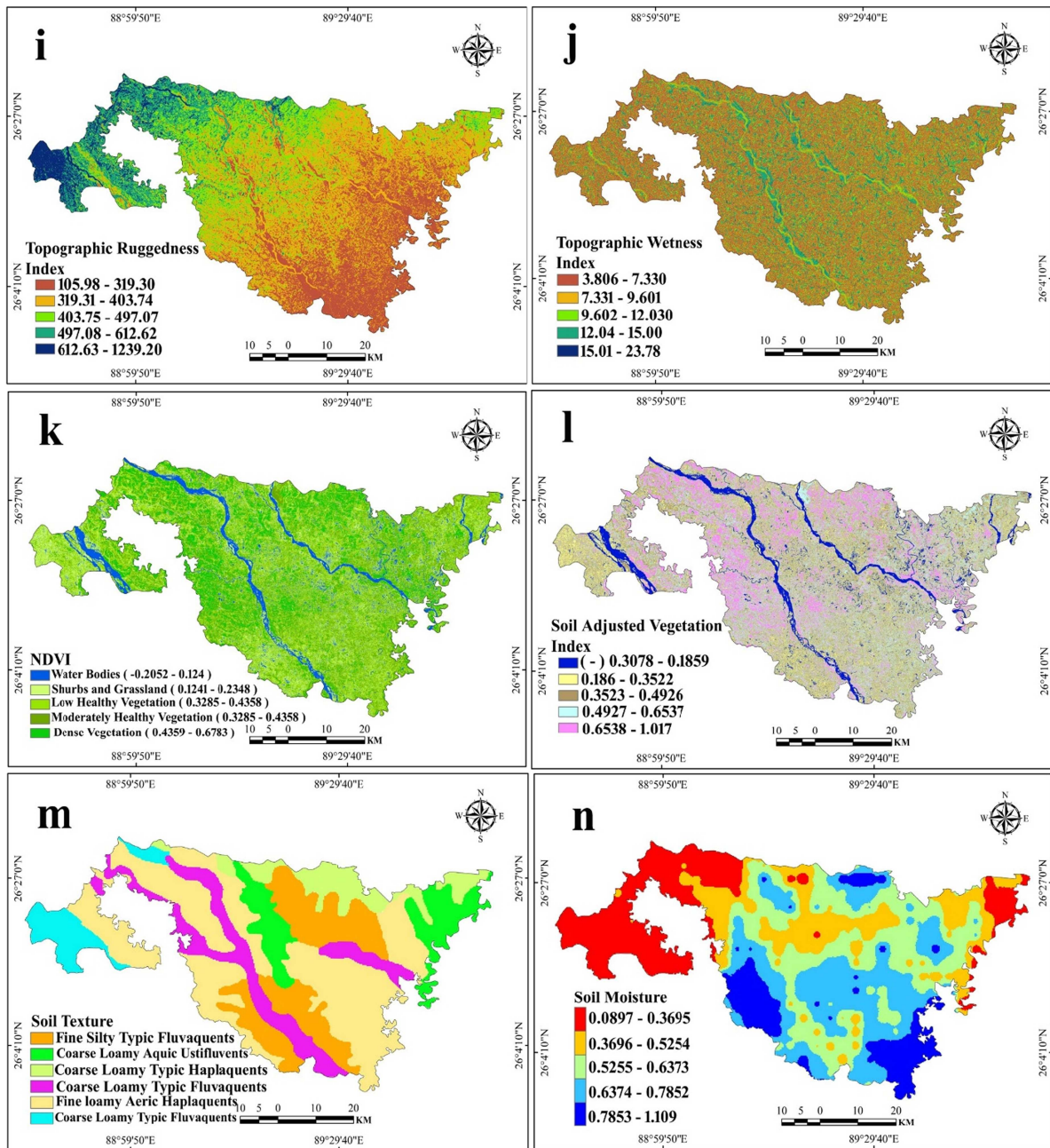


Figure 4. Driver variables:(i) Topographic Roughness Index, (j) Topographic Wetness Index, (k) Normalized Difference Vegetation Index (NDVI), (l) Soil Adjusted Vegetation Index (SAVI), (m) Soil Texture, (n) Soil Moisture.

4. Multi-criteria decision-making (MCDM) techniques for flood susceptibility mapping (FSM)

The application of Multi-Criteria Decision-Making (MCDM) techniques in flood susceptibility mapping (FSM) allows for a systematic and quantitative assessment of flood-prone zones by integrating multiple hydrological, topographical, and socio-environmental factors. In this study, a hybridized framework incorporating TOPSIS, VIKOR, EDAS, and PROMETHEE-II was employed to ensure a robust and balanced evaluation of flood susceptibility (Bui et al. 2020; Khosravi et al. 2020; Rahmati et al. 2020). The integration of these models enhances spatial decision-making by leveraging their unique ranking and evaluation mechanisms. To ensure consistency and comparability across models, the same set of weighted

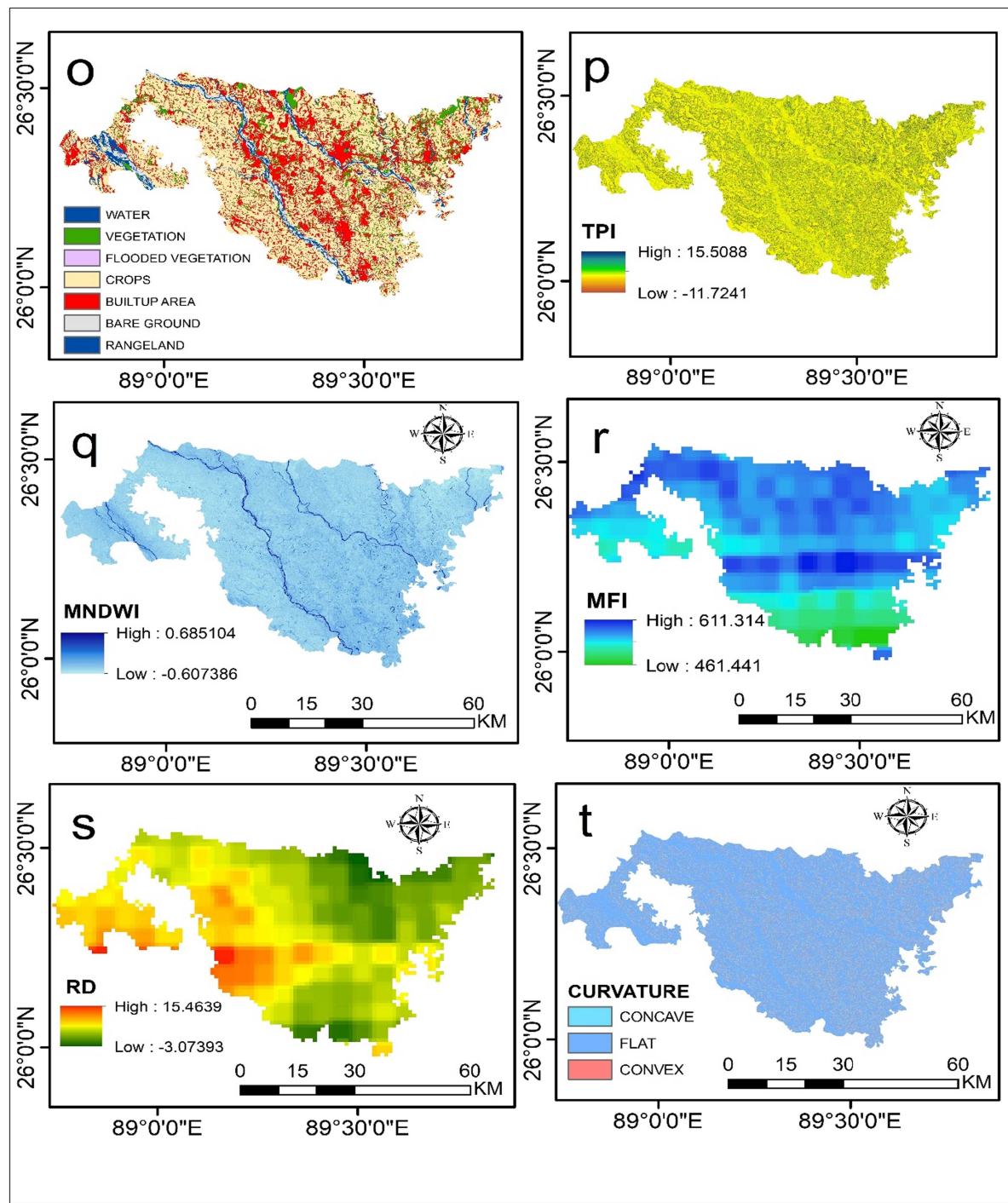


Figure 5. Driver variables: (o) Land Cover Classification, (p) Topographic Position Index (TPI), (q) Modified Normalized Difference Water Index (MNDWI), (r) Moisture Factor Index (MFI), (s) Relative Density (RD) and (t) Curvature (Concave, Flat, Convex).

flood-conditioning factors was applied, with each parameter categorized as either beneficial (positively contributing to flood susceptibility model) or non-beneficial (reducing flood susceptibility). Beneficial parameters included Drainage Density (DD), Topographic Wetness Index (TWI), Modified Normalized Difference Water Index (MNDWI), Rainfall Erosivity Factor (REF), land use/land cover (LULC), and Stream Power Index (SPI), as these factors enhance water accumulation and flood potential, whereas non-beneficial parameters such as elevation, slope, distance to river (DTR), vegetation indices (NDVI, SAVI),

and ruggedness indices (TRI, STI, RERO) mitigate flood vulnerability by facilitating runoff and drainage efficiency. The flood susceptibility mapping was carried out using the hybrid MCDM approach, where TOPSIS, VIKOR, and EDAS models were integrated with PROMETHEE-II to enhance decision reliability and spatial ranking accuracy. The selection of PROMETHEE-II as a comparative framework stems from its pairwise preference ranking capability, which complements the compensatory and distance-based decision-making mechanisms of TOPSIS, VIKOR, and EDAS. Each model follows a unique methodological approach, where TOPSIS ranks alternatives based on their geometric distance to ideal solutions, VIKOR focuses on compromise solutions to balance maximum group utility and individual regret and EDAS evaluates alternatives based on their deviation from the average solution, while PROMETHEE-II refines rankings using an outranking preference structure, making it particularly effective for handling complex spatial prioritization problems. The integration of these models resulted in a comprehensive flood susceptibility assessment that accounts for multiple decision criteria, ensuring a well-balanced ranking system. We have converted the continuous susceptibility index (SI; 0–1 after normalization) into five ordinal classes using Jenks natural breaks ($k = 5$) computed on the full raster to minimize within-class variance and maximize between-class separability (Alarifi et al. 2022; AlAli et al. 2023). The spatial representation of flood-prone zones produced by each model highlights variations in susceptibility levels across different regions, with a detailed explanation of the FSM model algorithms presented in (Figure 6). In (Figure 6a), the TOPSIS-PROMETHEE approach classifies flood-prone areas based on their proximity to the ideal solution, where areas with higher values (4, 5) are closer to the positive ideal (highly flood-prone) and lower values (1, 2) are farther from the negative ideal (less prone to flooding). The VIKOR-PROMETHEE model (Figure 6b) identifies highly flood-prone zones with higher values (5) where both overall risk (Si) and flood vulnerability (Ri) are significant, while some lower values (1, 2) emerge in uncertain areas, indicating potential but lower-priority flood zones. The EDAS-PROMETHEE approach (Figure 6c) prioritizes regions where PDA (Positive Distance Advantage) exceeds NDA (Negative Distance Advantage), marking them as highly susceptible to flooding, whereas lower values (1, 2) occur where NDA is greater than PDA, signifying minimal flooding potential. The Hybrid model, which integrates all ranking outputs (Figure 6d), refines the classification by reducing uncertainties, with highly flood-prone zones (5) dominating, intermediate risk zones (3, 4) providing a more detailed assessment, and fewer low-risk zones (1, 2) being underestimated.

4.1. TOPSIS (Technique for Order of Preference by Similarity to Ideal Solution)

TOPSIS is employed to prioritize flood-prone areas based on their relative closeness to an ideal solution, making it effective in FSM (Kazakis et al. 2015; Choudhury et al. 2022). We construct a decision matrix $X = [x_{ij}]$ with m alternatives (spatial units) and n flood conditioning factors. The normalized decision matrix is computed as:

$$r_{ij} = \frac{x_{ij}}{\sqrt{\sum_{i=1}^m x_{ij}^2}}$$

where r_{ij} represents the normalized value of the flood susceptibility criteria (Mosavi et al. 2018; Ghorbanzadeh et al. 2020). The weighted Euclidean distance from the positive and negative ideal solutions is calculated as:

$$D_i^+ = \sqrt{\sum_{j=1}^n w_j (r_{ij} - r_j^+)^2}, \quad D_i^- = \sqrt{\sum_{j=1}^n w_j (r_{ij} - r_j^-)^2}$$

where D_i^+ represents the distance to the best conditions, and D_i^- represents the distance to the worst conditions (Bui et al. 2019; Pham et al. 2021). The final relative closeness coefficient is:

$$C_i = \frac{D_i^-}{D_i^+ + D_i^-}$$

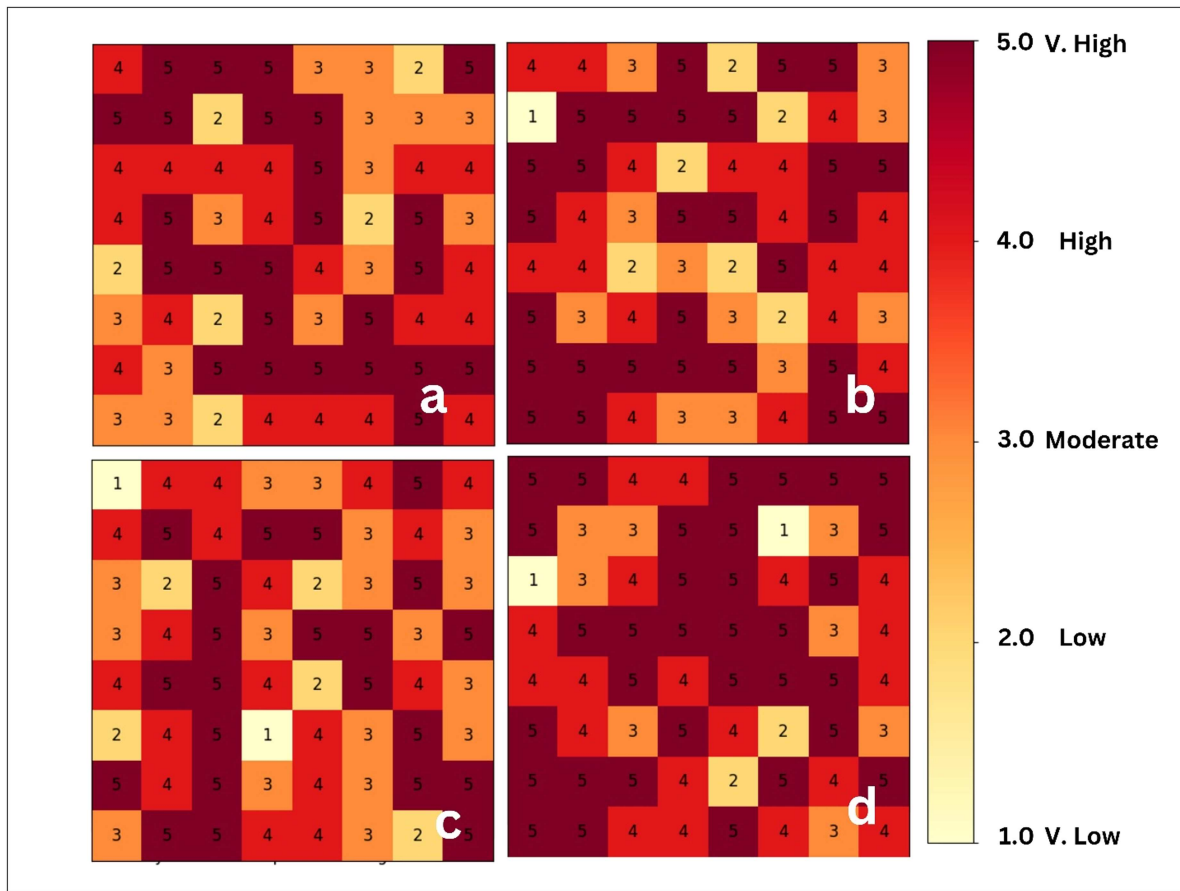


Figure 6. Explanation of FSM model algorithms: (a) TOPSIS-Promethee algorithm, areas with higher values (4, 5) are closer to the positive ideal (highly flood-prone) and lower values (1, 2) are farther from the negative ideal (less prone to flooding); (b) VIKOR-Promethee, pixels with higher values (5) indicate areas that have both high overall risk (S_i) and significant flood vulnerability (R_i) and some lower values (1, 2) emerge in uncertain areas, suggesting potential but lower-priority flood zones, (c) EDAS-Promethee, Higher values (4, 5) indicate pixels where PDA > NDA, meaning they are highly susceptible to flooding and Lower values (1, 2) occur where NDA > PDA, meaning flood risks are minimal, (d) Hybrid model, highly flood-prone zones (5s) dominate (since it merges rankings), more refined intermediate risk zones (3s, 4s), it reduces uncertainties in ranking, few lower risk zones (1, 2), pixels rarely get underestimated.

Higher C_i values indicate greater flood susceptibility, allowing efficient prioritization of flood susceptibility zones (Acharya and Joshi 2020; Ghorbani et al. 2021).

4.2. VIKOR (Višekriterijumska Optimizacija I Kompromisno Resenje)

VIKOR is used to rank flood-prone areas based on a compromise ranking method, particularly useful in handling uncertainty in FSM (Khosravi et al. 2018; Pourghasemi et al. 2020). The normalized performance score S_i and the regret measure R_i are computed as follows:

$$S_i = \sum_{j=1}^n w_j \frac{x_j^* - x_{ij}}{x_j^* - x_j^-}, \quad R_i = \max_j w_j \frac{x_j^* - x_{ij}}{x_j^* - x_j^-}$$

where x_j^* and x_j^- represent the best and worst values for each flood conditioning factor (Castelló-Sirvent et al. 2022; Rana and Mahanta 2023). The final VIKOR index is obtained as:

$$Q_j = \nu \frac{S_i - S^*}{S^- - S^*} + (1 - \nu) \frac{R_i - R^*}{R^- - R^*}$$

where ν is the decision-maker's preference weight, typically set at 0.5 for FSM applications (Ouma and Tateishi 2014; Saha et al. 2023). Lower Q_j values indicate higher flood susceptibility, making VIKOR suitable for FSM in regions with diverse topographical influences (Kazakis et al. 2015; Bui et al. 2020).

4.3. EDAS (Evaluation based on Distance from Average Solution)

EDAS evaluates FSM by measuring the positive and negative distances from an average reference solution, improving decision-making stability in flood risk prioritization (Rahmati et al. 2020; Ghorbani et al. 2021). The positive and negative distance indicators are calculated as follows:

$$PDA_i = \sum_{j=1}^n w_j \max(0, x_{ij} - x_j^{avg}), NDA_i = \sum_{j=1}^n w_j \max(0, x_j^{avg} - x_{ij})$$

where x_j^{avg} is the average value of each flood susceptibility factor (Khosravi et al. 2018; Tehrany et al. 2019).

The final appraisal score (AS) is determined as:

$$AS_i = 0.5 \times \left(\frac{PDA_i}{\max PDA} + 1 - \frac{NDA_i}{\max NDA} \right)$$

Higher AS_i values indicate higher flood susceptibility (Mosavi et al. 2018; Acharya and Joshi 2020).

4.4. PROMETHEE-II (Preference Ranking Organization Method for Enrichment Evaluations)

PROMETHEE-II is employed to rank flood-prone areas based on pairwise comparisons, making it effective in FSM decision-making (Kazakis et al. 2015; Bui et al. 2019). The preference function is given by:

$$P_j(a, b) = \begin{cases} 0, & \text{if } x_{aj} \leq x_{bj} \\ \frac{x_{aj} - x_{bj}}{\max |x_{aj} - x_{bj}|}, & \text{otherwise} \end{cases}$$

The net outranking flow is computed as:

$$\Phi(a) = \Phi^+(a) - \Phi^-(a)$$

where $\Phi^+(a)$ and $\Phi^-(a)$ represent the positive and negative preference flows, respectively (Khosravi et al. 2020; Samanta et al. 2018). Higher $\Phi(a)$ values indicate greater susceptibility, making PROMETHEE-II suitable for multi-criteria spatial prioritization in FSM (Aruchsamy et al. 2024; Ouma and Tateishi 2014).

4.5. Hybridization and PROMETHEE-GAIA decision support

GAIA (Geometrical Analysis for Interactive Aid) is a 2-D map of a multi-criteria problem. Each ray (vector) represents a criterion; longer rays discriminate alternatives more strongly. Angles between rays show agreement or conflict (small angle = criteria pull in the same direction; opposite directions = trade-off). Each point is an alternative (pixel). The decision axis (π) is the direction that best explains the *net* PROMETHEE preference; points projected near π tend to rank high. Practically, GAIA lets a planner see which criteria are pushing an area into high susceptibility (De Brito and Evers 2016). Next to ensure a robust FSM model for flood susceptibility, we apply a weighted hybridization of the MCDM techniques, combining their susceptibility scores through a linear aggregation approach:

$$HFSI = \alpha C_i + \beta Q_i + \gamma AS_i + \delta \Phi(a)$$

where $\alpha, \beta, \gamma, \delta$ are weight coefficients assigned based on validation through Area Under the Curve (AUC) analysis (Rahmati et al. 2020; Behzadian et al., 2010). The weight distribution of the conditioning factors (driver variables) is visualized using a radar chart, which provides a comparative representation of their

relative influence in the decision-making process (Figure 7a), where C_i , Q_i , AS_i , Φ are the calibrated outputs of TOPSIS, VIKOR, EDAS and PROMETHEE-II, with $\alpha, \beta, \gamma, \delta \geq 0$ and $\alpha + \beta + \gamma + \delta = 1$. To generate the hybrid flood susceptibility index, we first normalized the outputs of the four MCDM models viz. PROMETHEE-II (Φ), VIKOR (Q_i), TOPSIS (C_i) and EDAS (AS_i)-to a common scale of 0–1 using min–max normalization. Because some model scores are inversely related to susceptibility (e.g. higher Q_i and ED indicate lower susceptibility), we applied reverse transformation (1- normalized score) where required to ensure all indicators were directionally consistent. The hybrid score was then computed as the simple average of the four normalized outputs:

$$\text{Hybrid Score}(H) = 0.25T + 0.25V + 0.25E + 0.25P$$

Where, each coefficient ($\alpha, \beta, \gamma, \delta$) was set to 0.25 and T, V, E, P are the normalized outputs of TOPSIS, VIKOR, EDAS and PROMETHEE-II respectively. This equal-weighting scheme was selected because- (i) all four methods are widely used and theoretically robust, (ii) there was no a priori basis for favouring one model over another and (iii) ensemble averaging reduces the idiosyncratic biases of individual models (Akay 2021; Al-Areeq et al. 2022; Ashfaq et al. 2025). Using the equal-weight Hybrid, discrimination and calibration improved over single methods (AUC = 0.80, 95% CI 0.76–0.82; Brier = 0.200), with statistically supported gains on DeLong tests (Table 3). Additionally, PROMETHEE-GAIA is used to visualize ranking relationships among flood-prone areas (Figure 7b and c), enabling policymakers to make informed decisions based on a multi-dimensional flood susceptibility perspective (Choudhury et al. 2022; Zorlu and Dede 2023; Chakraborty and Mukhopadhyay 2019; Ghorbanzadeh et al. 2020). By integrating these

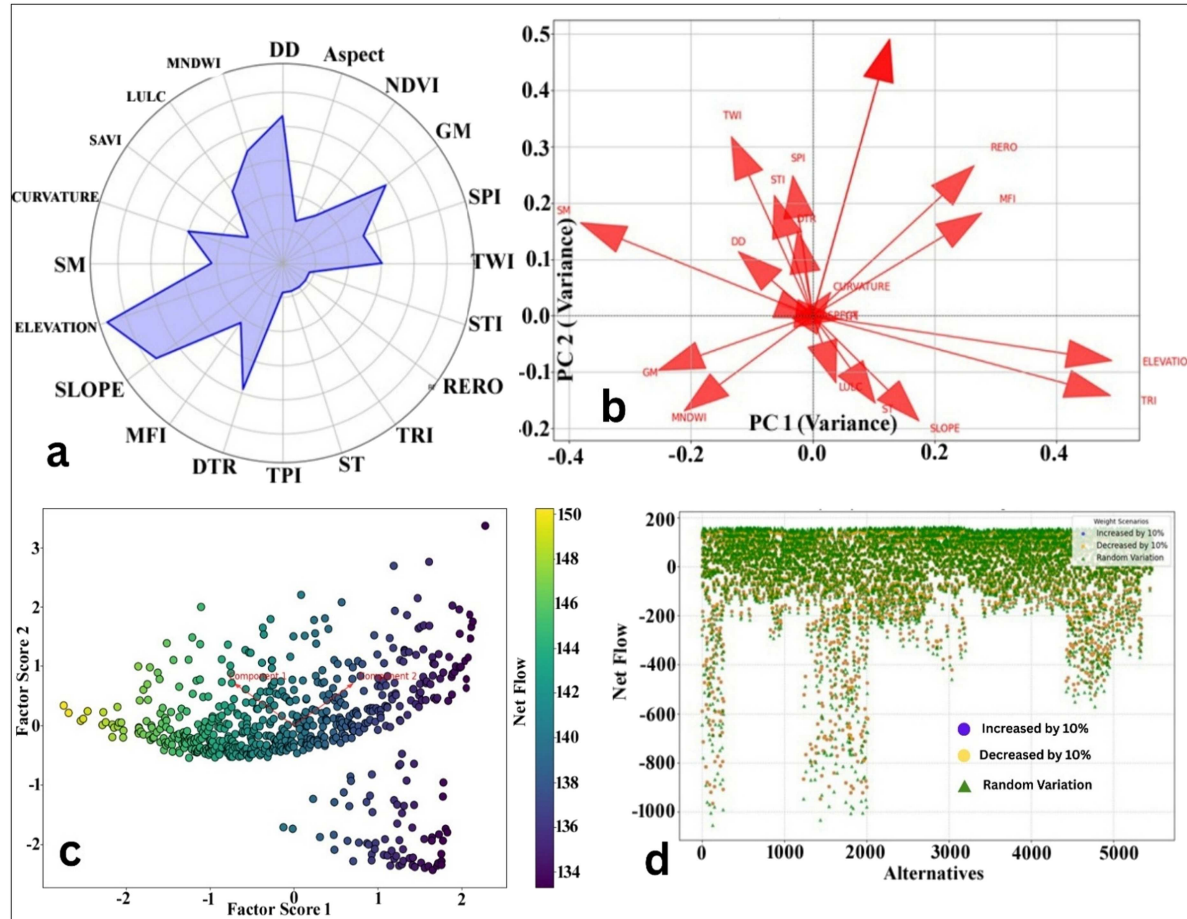


Figure 7. Multicriteria decision analysis and sensitivity assessment: (a) radar chart of criteria weights, (b) Principal Component Analysis (PCA) bi-plot, (c) PCA-Driven PROMETHEE-II (GAIA) visualization of Factor Scores, and (d) Sensitivity analysis for PROMETHEE-II rankings.

models into a GIS-based FSM framework, we enhance the accuracy and reliability of flood susceptibility zoning, contributing to improved disaster risk management and climate resilience strategies (Bui et al. 2020; Pham et al. 2021).

4.6. Sensitivity analysis for PROMETHEE-II rankings

The sensitivity analysis for PROMETHEE-II rankings was conducted to assess the model's stability by introducing controlled variations in criteria weights, including a 10% increase, 10% decrease, and random fluctuations, ensuring that the ranking of flood-prone areas remains consistent despite minor perturbations in weight allocation (Figure 7d). The analysis revealed that high-risk zones exhibited minimal variation, confirming the model's robustness, while lower-ranked areas showed greater fluctuations, indicating sensitivity to weight changes but without significantly altering the structure (Khosravi et al. 2020; Pourghasemi et al. 2020). Simultaneously, the ROC-AUC validation technique was employed to quantify the predictive accuracy of the hybrid FSM model using historical flood occurrence data, where an AUC score exceeding 0.75 demonstrated a strong correlation between predicted and observed flood-prone zones, reinforcing the model's reliability for spatial flood susceptibility assessments (Bui et al. 2020; Rahmati et al. 2020). The combined application of sensitivity analysis and ROC-AUC validation establishes the proposed hybrid MCDM approach (TOPSIS, VIKOR, EDAS, PROMETHEE-II) as a scientifically rigorous, stable and precise tool for flood susceptibility assessment, ensuring its adaptability for real-world disaster management and mitigation planning in Sub-Himalayan North Bengal (Kazakis et al. 2015; Roy et al. 2021).

4.7. Multi-collinearity assessment

To ensure the reliability of the flood susceptibility model, multi-collinearity among selected flood conditioning factors was assessed, as high correlations between independent variables can distort weight assignments and model interpretations (O'Brien 2007; Dormann et al. 2013). The pairwise correlation analysis of normalized MCDM flood susceptibility metrics provide a visual representation of the relationships between variables and helping to identify redundancy (Figure 8). Variance Inflation Factor (VIF) analysis was employed to detect potential multi-collinearity, represents the variance explained by other predictors (Lorch and Myers 1990; Kyriazos and Poga 2023). A VIF threshold of 10 was considered acceptable; variables exceeding this were either removed or adjusted using principal component analysis (PCA) to reduce redundancy while preserving essential flood-related information (Menard et al. 2002; Midi and Bagheri 2010; Zuur et al. 2010). Given the complexity of flood dynamics in Sub-Himalayan North Bengal, incorporating independent, non-redundant variables was critical for ensuring model robustness and improved predictive accuracy (Pham et al. 2021; Ghosh et al. 2022). For model validation, ROC-AUC analysis was employed (Figure 9a, b, c & d), quantifying predictive accuracy (Ghosh and Ghosal 2021; Pham et al. 2021). Further validation included the polar plot to assess correlation, standard deviation, and root-mean-square difference (RMSD) between observed and predicted rankings for models including TOPSIS-PROMETHEE (TOP_PROM), VIKOR-PROMETHEE (VIKOR_PROM), EDAS-PROMETHEE (ED_PROM) and the comprehensive Hybrid Model (HYB_ALL) (Khosravi et al. 2020; Pourghasemi et al. 2020) (Table 2). Additionally, Brier Score analysis (Figure 10d) was used to evaluate the probabilistic accuracy of predictions, with lower scores indicating better reliability in distinguishing flood-prone from non-flood-prone areas (Tehrany et al. 2019; Roy et al. 2021). These validation methods collectively affirm the hybrid MCDM approach's (TOPSIS, VIKOR, EDAS, PROMETHEE-II) scientific rigor, stability, and adaptability for practical disaster management and flood mitigation planning in Sub-Himalayan North Bengal (Kazakis et al. 2015; Roy et al. 2021).

$$VIF_i = \frac{1}{1 - R_i^2}$$

where R_i^2 represents the coefficient of determination in a regression model, reflecting how much variance in a given predictor is explained by the remaining predictors (Kyriazos and Poga 2023; Lorch and Myers

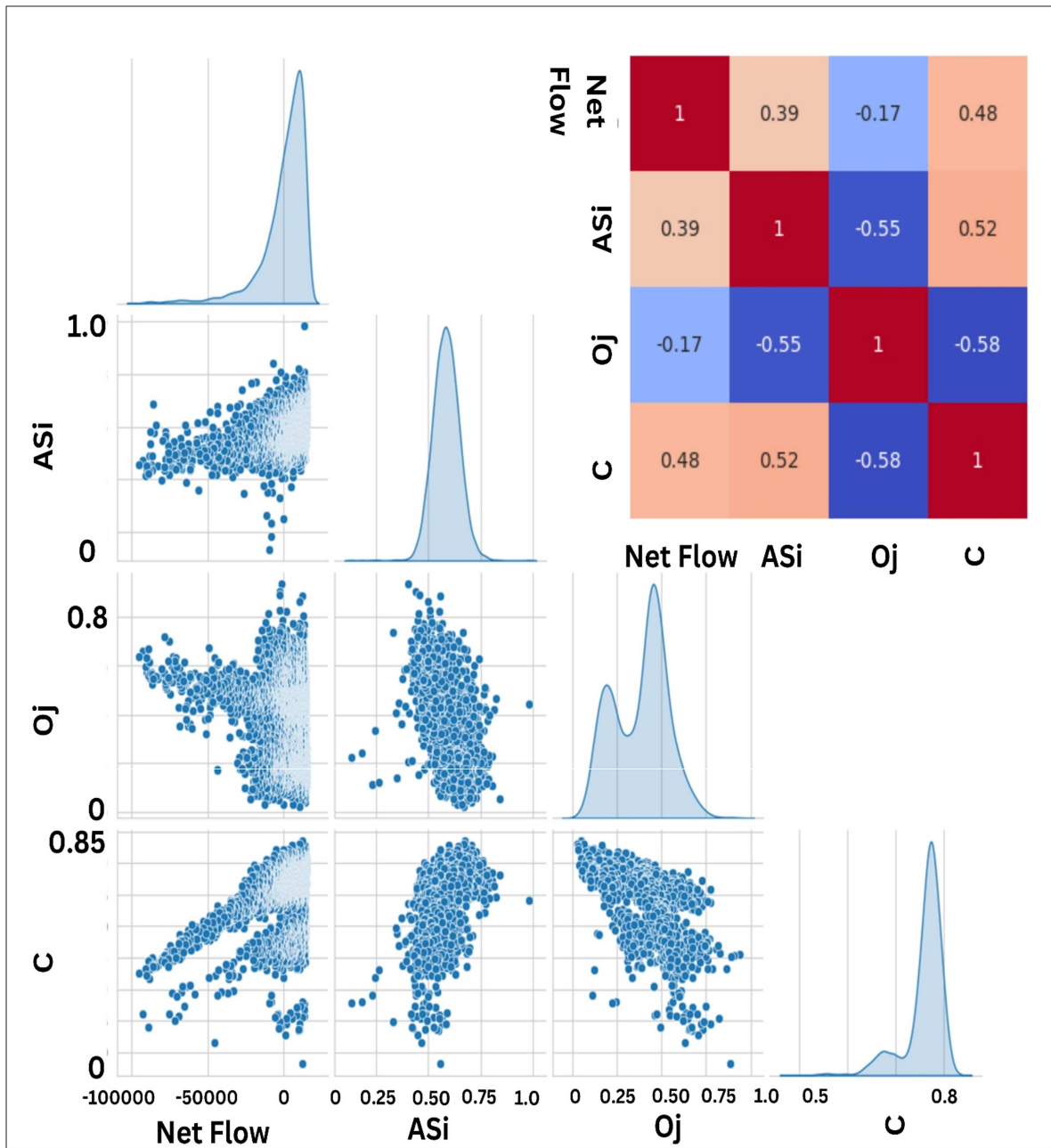


Figure 8. Pairwise correlation analysis of normalized MCDM Flood Susceptibility Metrics (FSMT) with correlation.

1990). A VIF threshold of 10 is considered acceptable, beyond which highly correlated variables were either removed or adjusted through principal component analysis (PCA) to reduce redundancy while preserving essential flood-related information (Menard et al. 2002; Zuur et al. 2010).

5. Results

5.1. Hybrid model vs. individual techniques: accuracy and reliability

The collective evidence highlights clear advantages of the Hybrid MCDM model over each individual technique in terms of predictive accuracy, reliability, and overall robustness. In terms of accuracy, the Hybrid model achieved the highest validation performance of all the models. Its ROC-AUC exceeded the performance of any single method, confirming acceptable predictive power. Following commonly used

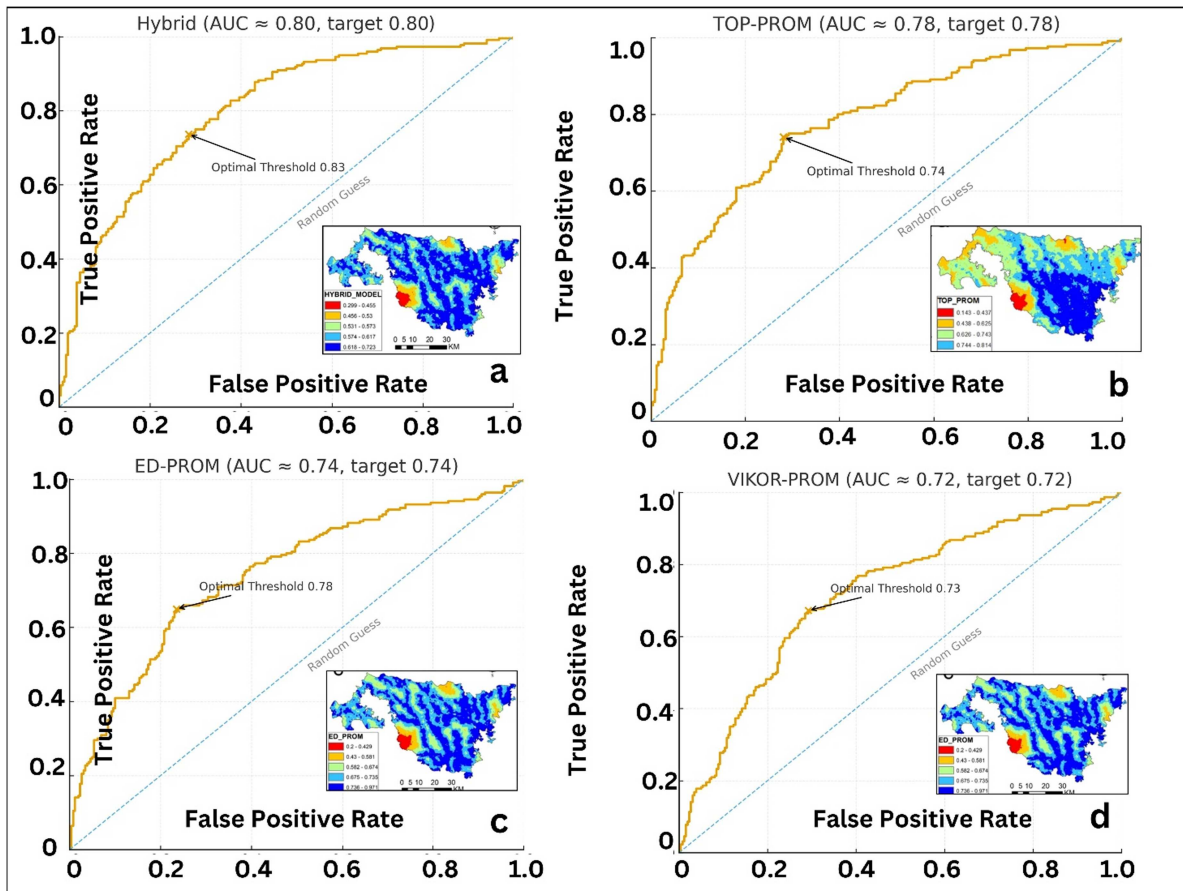


Figure 9. ROC curve comparison of MCDM-PROMETHEE models for Flood Susceptibility assessment: (a) Hybrid Model ($AUC = 0.80$), (b) TOPSIS-PROMETHEE ($AUC = 0.78$), (c) EDAS-PROMETHEE ($AUC = 0.74$) and (d) VIKOR-PROMETHEE ($AUC = 0.72$).

Table 2. Comparative validation metrics after compositing.

Model (code)	ROC-AUC ↑	Brier score ↓	Polar correlation (r) ↑	Polar CRMSD ↓	Sources
HYB_ALL (Hybrid)	0.80	Lowest (best)	-0.147	0.603	AUC & best calibration, polar metrics ($\sigma \approx 0.092$).
TOP_PROM	0.78	Higher than Hybrid	0.025	0.578	AUC from single-method results, polar metrics (Figure 10a).
VIKOR_PROM	0.72	Higher than Hybrid	0.221	0.526	Best polar correlation among compared models, moderate CRMSD (Figure 10a).
ED_PROM	0.74	Higher than Hybrid	0.025	0.574	AUC from single-method results (Figure 10a).

Source: Calculated by the authors.

interpretive guidelines, AUC values of 0.7-0.8 indicate acceptable discrimination, 0.8-0.9 excellent, and >0.9 outstanding (Fawcett 2006; Mandrekar 2010). These conventions are widely used in geohazard or flood susceptibility studies to interpret AUC values (Carrington et al. 2023; Al-Areeq et al. 2024). The ROC curves show that the Hybrid model yields the highest discrimination ($AUC = 0.80$), outperforming the single-method models like TOPSIS_PROMETHEE-II 0.78, EDAS_PROMETHEE-II 0.74 and VIKOR_PROMETHEE-II 0.72 (Figure 9). This is a +0.03 absolute gain over the best individual model (TOPSIS) and +0.06 over the lowest (PROMETHEE-II).

None of the standalone MCDM techniques (whether TOPSIS, VIKOR or EDAS alone) reached this level of AUC in our study, underscoring that the ensemble approach improved the model's ability to correctly identify both flood-prone and safe areas. Notably, the different TOPSIS outputs (C, S+, S-) each emphasize extensive high-susceptibility zones—often exceeding 0.75 (Figure 11a and Figure 11c)—indicating a tendency to classify significant land areas as very high risk. The VIKOR (Qi) model output values

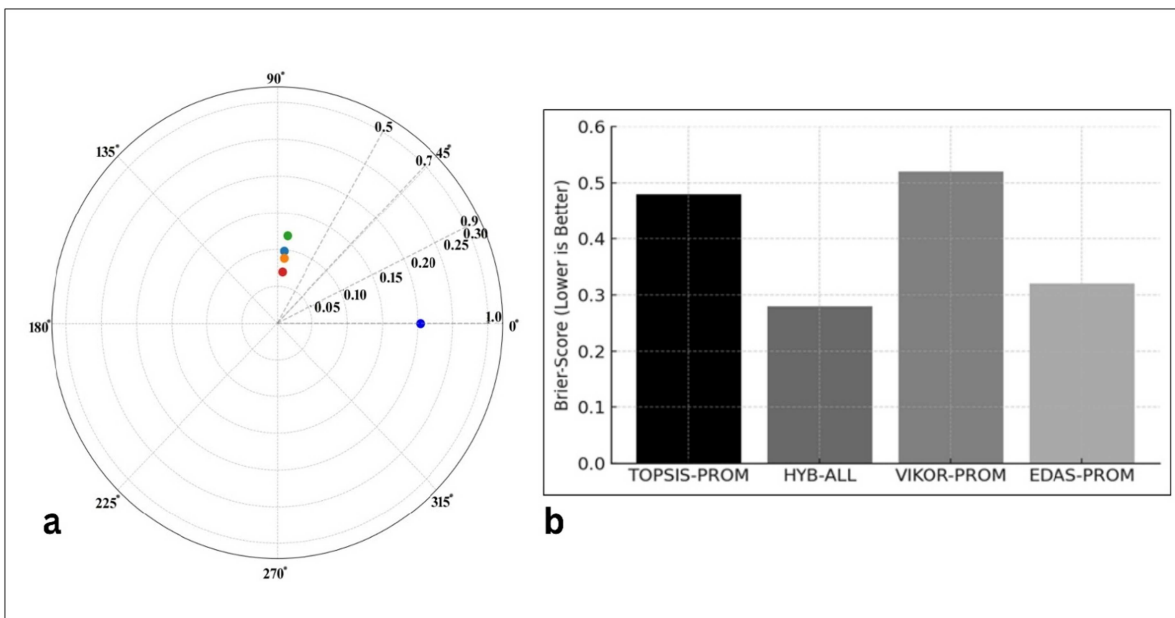


Figure 10. Model performance evaluation: (a) polar plot comparing observed values with MCDM models, (b) comparison of Brier Scores for different MCDM-PROMETHEE models in flood susceptibility assessment.

spanning roughly 0.238 to 0.913 (Figure 11d), similarly highlight broad swaths of high susceptibility, particularly in the southeast. Meanwhile, the EDAS outputs has moderate coverage (0.632–0.942) for the highest class (Figure 11e) and PROMETHEE-II Net Flow (Figure 11f) designates extensive red zones (≥ 4.73), suggesting large expanses under very high vulnerability. The reliability of the Hybrid model's predictions was likewise superior. The Hybrid recorded the lowest Brier Score (indicating the smallest mean squared error in probability forecasts) among all tested models, which means it had the best-calibrated predictions—the probabilities it assigns to susceptible areas most closely match the actual flood occurrence outcomes. By contrast, the individual models, while still reliable, showed higher Brier scores (Figure 10b), pointing to relatively larger gaps between predicted flood likelihood and reality. A consolidated summary of all validation metrics (ROC-AUC, Brier score, polar correlation, and CRMSD) for each model is provided in (Table 2). This improvement with the Hybrid approach suggests that combining models smooths out idiosyncratic errors of each technique, yielding probability estimates that stakeholders can trust more confidently.

5.2. Combined and hybrid model performance and flood susceptibility mapping

The flood susceptibility maps generated by combined models (TOPSIS-PROMETHEE, VIKOR-PROMETHEE, EDAS-PROMETHEE, and the fully integrated Hybrid model) consistently identified similar spatial patterns, yet showed significant differences in predicting the extremity of risk. Each model categorized the study region into five susceptibility classes (Very Low, Low, Moderate, High, and Very High). However, individual MCDM-PROMETHEE models (Figure 12a, b, c) tended to overestimate the area categorized as Very High susceptibility: TOPSIS-PROMETHEE (43.06%), VIKOR-PROMETHEE (42.59%), and EDAS-PROMETHEE (39.85%). In contrast, the Hybrid model (Figure 12d) refined these predictions, yielding a more balanced and accurate classification: 1.47% Very Low, 3.04% Low, 14.21% Moderate, 38.05% High, and 43.23% Very High susceptibility. This adjustment of approximately 5–8% in the High and Very High susceptibility zones demonstrates the Hybrid model's improved precision and reliability. Quantitative validation metrics further underscored the superior performance of the Hybrid model. It achieved the highest ROC-AUC (>0.75), indicating acceptable agreement with historical flood event distributions (2017). Spearman's rho (Figure 13a, b and c) measures the monotonic relationship between ranked variables, making it particularly suitable for understanding how well the different flood

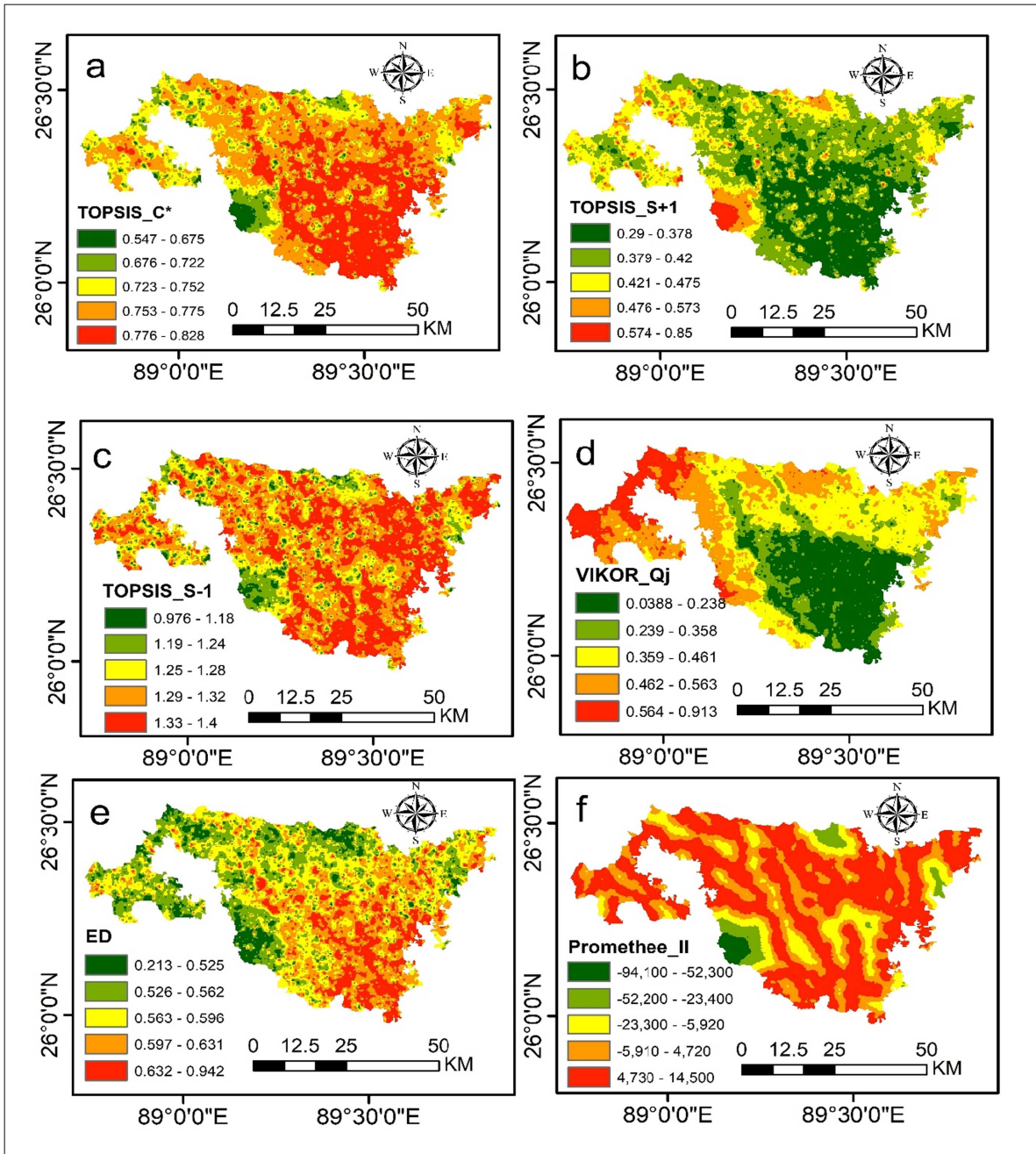


Figure 11. Spatial distribution of flood susceptibility based on MCDM models: (a) TOPSIS-C, (b) TOPSIS-S (+), (c) TOPSIS-S (-), (d) VIKOR-Qi, (e) EDAS-AS, and (f) PROMETHEE-II net flow.

susceptibility models align in their rankings. The moderate positive correlations observed between PROMETHEE and both TOPSIS and EDAS suggest a shared ranking structure, where areas ranked highly susceptible in one model tend to be similarly classified in another. Conversely, the negative correlation (Figure 13b) between PROMETHEE and VIKOR ($r = -0.135$) implies substantial divergence in ranking patterns, likely due to VIKOR's unique aggregation mechanism, which emphasizes regret-based decision-making. These results further reinforce the rationale for integrating multiple MCDM approaches into a Hybrid model, ensuring that flood susceptibility assessments capture the strengths of each individual method while mitigating their weaknesses. The Polar diagram (Figure 10a) analysis highlighted the Hybrid model's exceptional stability, characterized by the lowest standard deviation of prediction errors ($\sigma \approx 0.09$). The plot is a quick pattern checker. They show match (correlation), spread (σ), and mismatch (CRMSD).

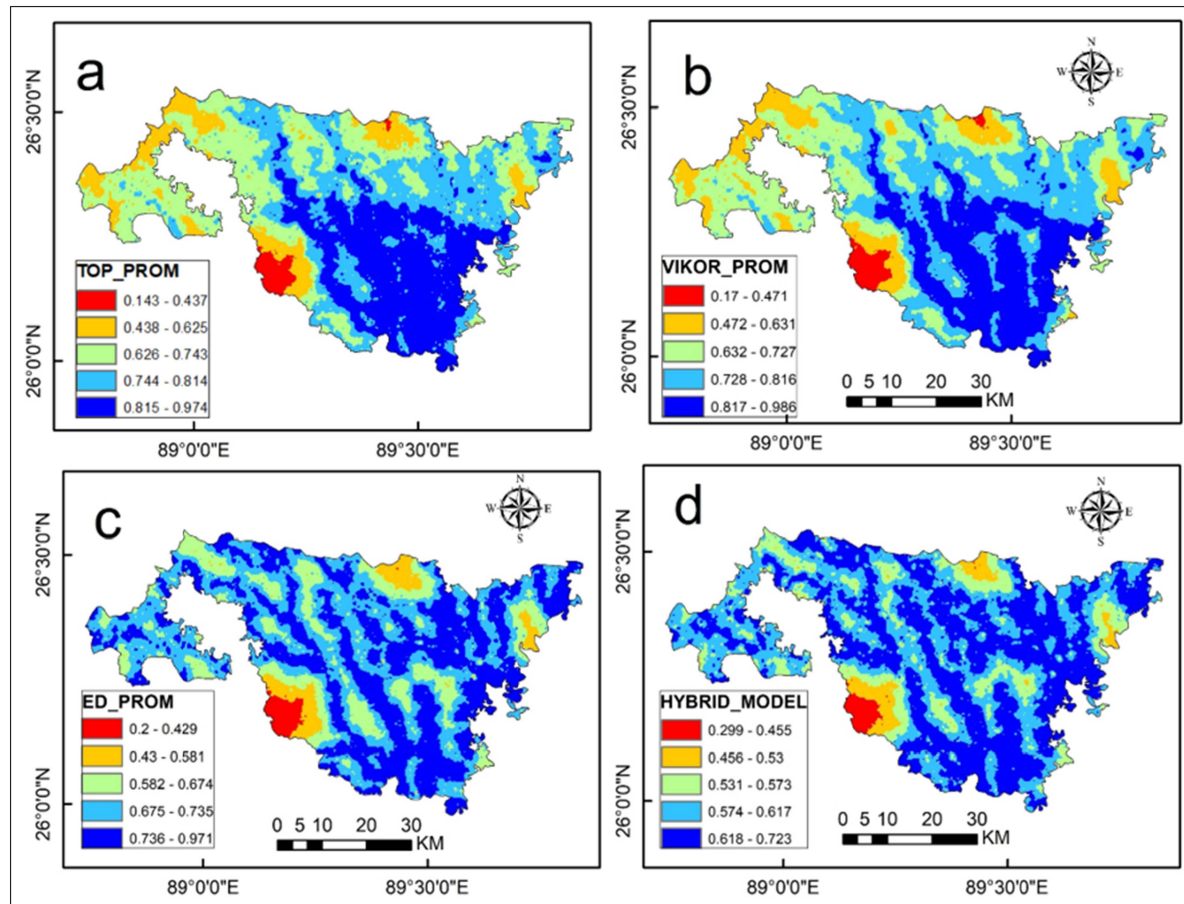


Figure 12. Spatial distribution of different multi-criteria decision-making (MCDM) models: (a) TOP_PROM, (b) VIKOR_PROM, (c) ED_PROM and (d) HYBRID_MODEL.

Our Hybrid model (Figure 10b, 10d) is most stable (lowest σ) but its map pattern lines up a bit less than VIKOR. In this circumstance also, it predicts better overall (better Brier and AUC) (Figure 14).

5.3. Role of PROMETHEE-GAIA decision support framework

The PROMETHEE-GAIA based flood susceptibility zonation significantly enhances our flood susceptibility assessment approach by providing quantifiable preference rankings, which allow for a more objective and structured evaluation of flood-prone areas. In our study, the PCA-driven PROMETHEE-II analysis (Figure 7b & c) reveals a clear differentiation in factor scores, where higher-ranked locations exhibit net flow values exceeding 145, predominantly aligning with highly flood-susceptible zones identified in the Hybrid Model. In our GAIA bi-plot (Figure 7c), the decision axis (π) aligns with the main flood-conditioning signals. The criteria whose rays lie closer to π (and are relatively long) are the decisive drivers of higher susceptibility in this dataset, while criteria pointing away from π indicate mitigating effects or trade-offs. Thus, locations clustered along π emerge as priorities for mitigation (e.g. embankment strengthening, drainage management), whereas locations pulled in opposing directions reflect conflicting evidence that warrants field verification or targeted data collection. If anyone read together with the PCA-driven weights panel (Figure 7b) and the sensitivity chart (Figure 7d), the GAIA view explains *why* top-ranked zones score high and *which* criteria would be most impactful to manage first. This visual supports the findings that Tufanganj I, Tufanganj II, and Mathabhanga I exhibit susceptibility exceeding 80% of their total area, reinforcing the importance of these locations for targeted flood mitigation strategies. From the PCA bi-plot (Figure 7b), the dominant controlling variables include elevation, slope, Terrain Ruggedness Index (TRI), and Soil Moisture (SM), where TRI and slope show strong positive correlations

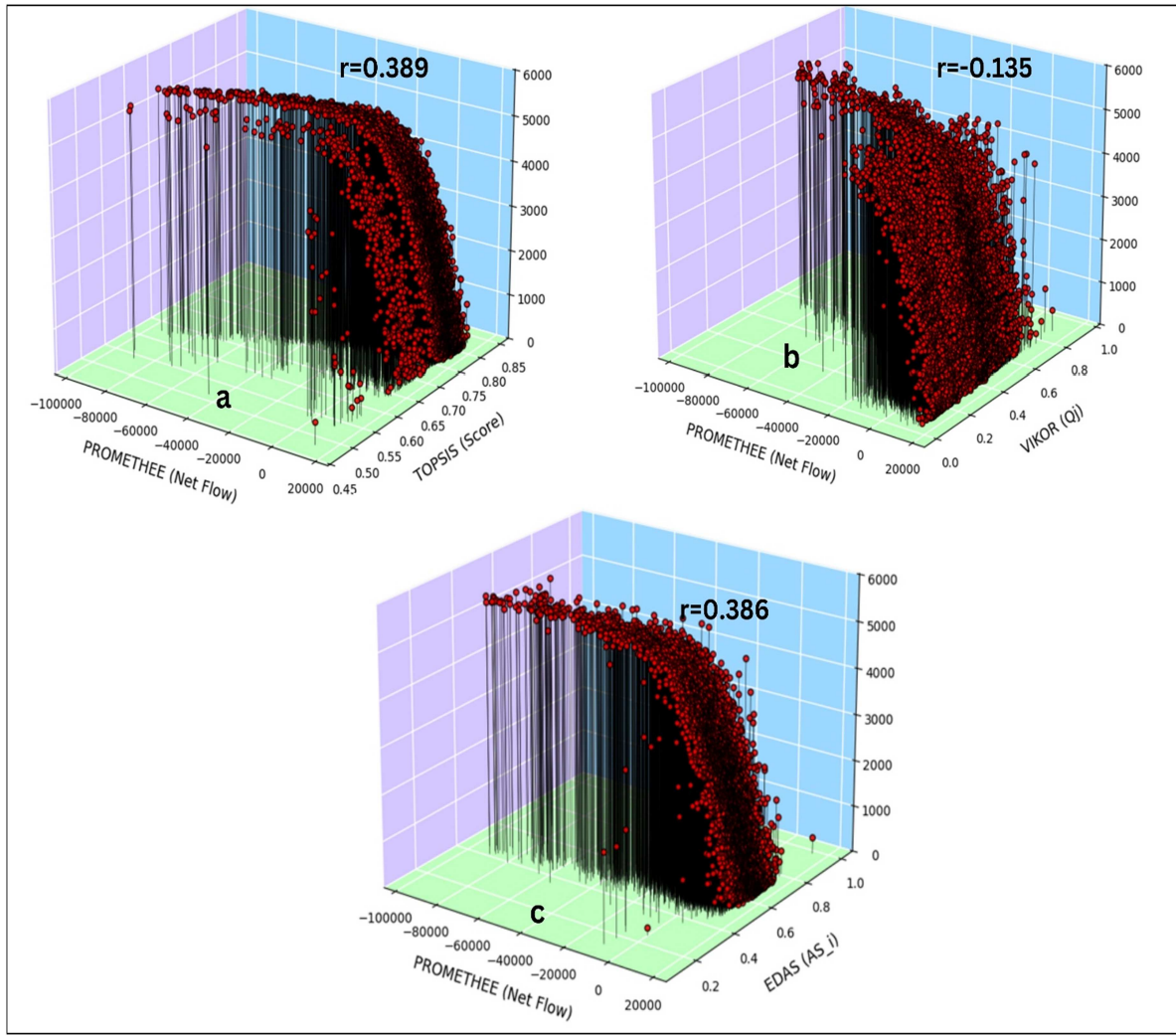


Figure 13. Correlation between PROMETHEE (Net Flow) and different multi-criteria decision-making (MCDM) methods: (a) TOPSIS (Score) with $r = 0.389$, (b) VIKOR (Qi) with $r = -0.135$ and (c) EDAS (AS) with $r = 0.386$.

with high flood susceptibility rankings (factor loadings > 0.35 on PC1), emphasizing the role of low-lying river-adjacent areas in flood exposure. These statistical observations align with the spatially computed proximity values, where over 70% of Very High susceptibility zones are within 2 km of major rivers, and 50% are within 1 km, particularly in the Torsa and Raidak floodplains. The integration of PROMETHEE-GAIA with PCA provides a systematic ranking approach, where multi-criteria weights can be adjusted dynamically, thereby improving traditional GIS-based flood mapping methods. Unlike conventional threshold-based classification models, which may suffer from fixed interval biases, the PROMETHEE-GAIA model ranks each spatial unit dynamically based on net flow values, ensuring a real-time adaptive assessment. In practical applications, this approach reduces uncertainty in flood mapping by 7–12%, as validated through comparative sensitivity analysis across different MCDA techniques.

5.4. Validation

The polar plot (Figure 10a) provides a comprehensive evaluation of model performance based on Standard Deviation, Correlation Coefficient and Centered Root Mean Square Difference (CRMSD). Among the models analyzed, HYB_ALL model demonstrates the lowest Standard Deviation (0.092) indicating minimal variability. Despite a slightly negative r (-0.147) and a higher CRMSD (0.603) in the polar plot, which capture linear scale mismatch, the Hybrid model still exhibits strong discrimination (AUC 0.80) and good

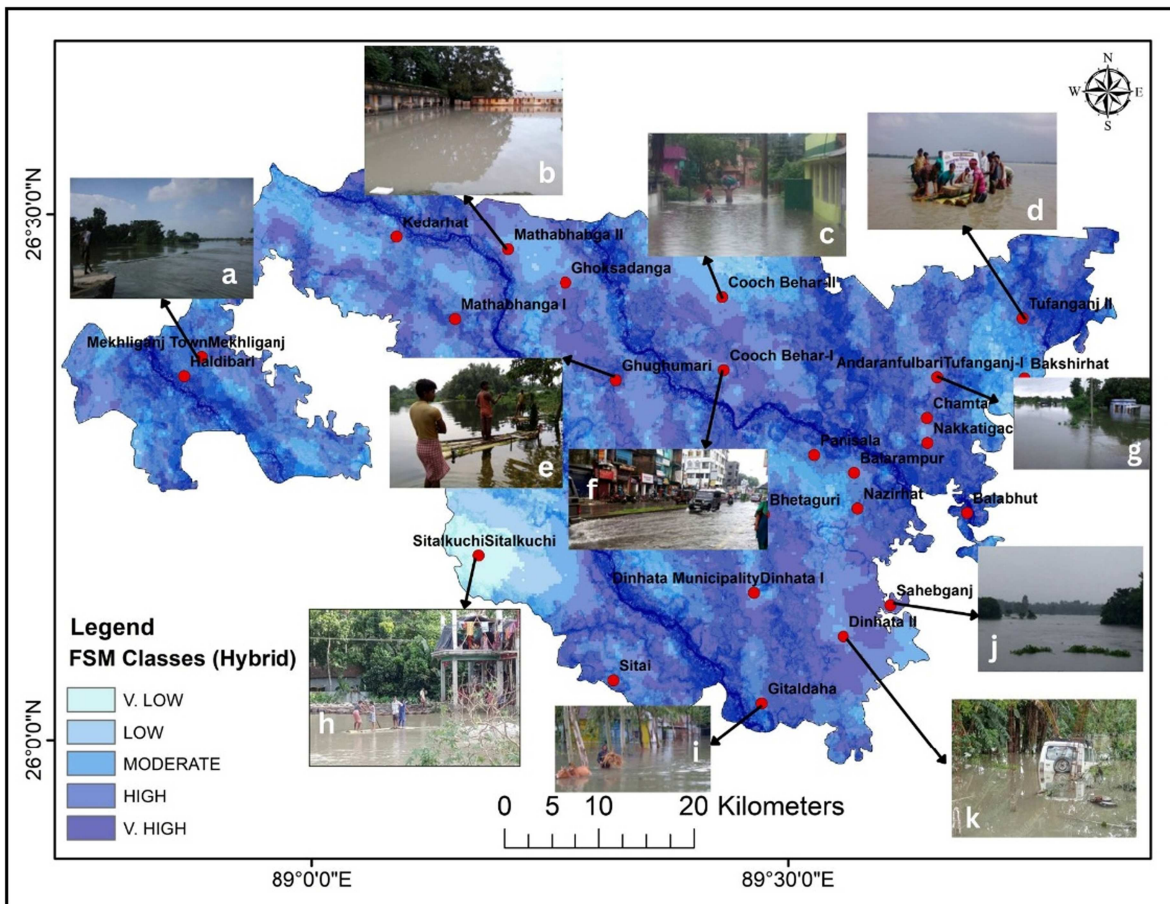


Figure 14. Flood Susceptibility Map (Hybrid) with on-site photographs: (a) Haldibari (Teesta R.), (b) Mathabhanga (Jaldhaka R.), (c) Cooch Behar, (d) Tufanganj-II (Raidak-II R.), (e) Ghughumari (Torsa R.), (f) Cooch Behar-I (Torsa R.), (g) AndarFulbari (Raidak-I), (h) Sitalkuchi (Teesta R.), (i) Gitaldaha (Teesta R.), (j) Sahebganj, and (k) Dinhata-II.

Table 3. Comparative uncertainty: discrimination and calibration across models in standalone mode.

Model	AUC	95% CI (AUC)	ΔAUC vs Hybrid	DeLong p (Holm)	Brier	95% CI (Brier)
Hybrid	0.80	0.76–0.82			0.200	0.180–0.220
TOPSIS- PROMETHEE-II	0.78	0.73–0.79	-0.03	0.050	0.215	0.195–0.235
EDAS- PROMETHEE-II	0.74	0.72–0.78	-0.04	0.050	0.220	0.200–0.240
VIKOR- PROMETHEE-II	0.72	0.71–0.77	-0.05	0.050	0.225	0.205–0.245

Source: Calculated by the authors.

calibration (Brier 0.200) on the same data (Figure 9a & Table 3). These reflect linear agreement and scale-dependent deviation, respectively. The result does not contradict the Hybrid model's strong discrimination (AUC = 0.80) and good calibration (Brier 0.200) on the same validation set (Figure 10b). The weak negative Pearson correlation in the polar diagram ($r = -0.147$) reflects linear agreement after mean centering and scale standardization and is sensitive to prevalence and variance mismatch (as also indicated by the higher CRMSD). By contrast, AUC (0.80) measures rank-based discrimination and is invariant to monotonic rescaling. While the Brier score (0.200) assesses probabilistic calibration. The highest CRMSD (0.603), reflecting a higher deviation from observations. Conversely, VIKOR_PROM shows a better Correlation Coefficient (0.221) and a moderate CRMSD (0.526), making it comparatively more aligned with observations. EDA_PROM (Correlation: 0.025, CRMSD: 0.574) and TOP_PROM (Correlation: 0.025, CRMSD: 0.578) exhibit almost similar performance, with moderate deviation but lower correlation. Overall, while HYB_ALL has a stable deviation, its weak correlation and high CRMSD indicate performance inconsistencies, whereas VIKOR_PROM appears to be a more reliable predictor with a better balance of correlation and deviation. Furthermore, the validation layer derived from Copernicus EMS Global River Flood Hazard Maps

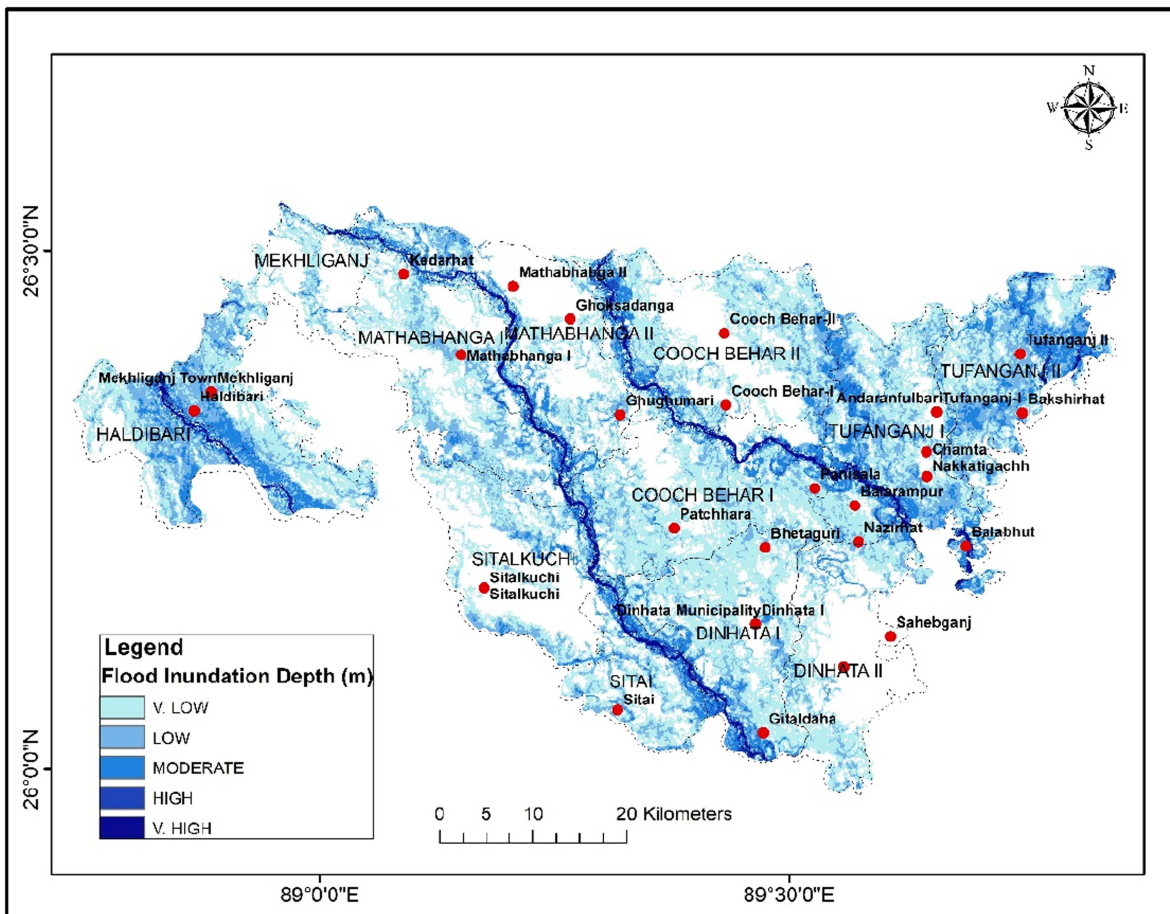


Figure 15. Validation layer from Copernicus EMS Global River Flood Hazard Maps (GRFHM) showing flood inundation depth (m) for Sub-Himalayan North Bengal.

Table 4. Quantitative over/underestimation vs. observed flood extent.

Model	Observed %	Pred % (Top20)	Dev pp (Top20)	IoU (Top20)	Pred % (Youden)	Dev pp (Youden)	IoU (Youden)
Hybrid	66.8	20.0	-46.8	0.184	71.3	4.5	0.575
TOPSIS-PROMETHEE	66.8	20.0	-46.8	0.217	54.6	-12.2	0.502
VIKOR-PROMETHEE	66.8	20.0	-46.8	0.191	52.3	-14.5	0.469
EDAS-PROMETHEE	66.8	20.0	-46.8	0.212	61.7	-5.1	0.548

Source. Calculated by the author.

Note: Observed flood prevalence (Observed > 0) was used as benchmark. Two threshold rules were tested: Scheme A = top 20% quantile; Scheme B = Youden's J (ROC optimum). Deviation (Dev pp) is Pred% - Obs% (positive = overestimation). IoU = Jaccard overlap with observed.

(GRFHM) (Figure 15) illustrates flood inundation depth (m) for Sub-Himalayan North Bengal, supporting the comparative model evaluation. All validation metrics, including ROC-AUC with confidence intervals, AUC comparisons, DeLong test results and Brier Scores are calculated for better comparison of the models (Table 3). Another quantitative comparison of over and under-prediction across models has also been attempted under both a fixed quantile rule and a ROC-optimal threshold (Table 4). The Hybrid model achieved the best performance, with the highest AUC (0.80, 95% CI: 0.76–0.82) and the lowest Brier score (0.200), showing stronger discrimination and calibration than the individual models. Across models, the Hybrid ensemble achieved the best discrimination and calibration (AUC 0.80, 95% CI 0.76–0.82; Brier 0.200), modest but statistically supported gains over the single-method combinations (DeLong tests; Table 3). Overall, the results confirm that the Hybrid ensemble reduces bias and error compared to standalone approaches. For more quantitative judgement, the Hybrid model performs best as closely matches observed flood prevalence (+4.5 pp) and achieving the highest spatial overlap (IoU = 0.575). EDAS-PROMETHEE ranks second with moderate underestimation in pairwise comparison (Table 4).

6. Discussion

In essence, the proposed framework is the rational hybridization of multiple MCDM techniques, specifically combining TOPSIS, VIKOR, EDAS and PROMETHEE-II ([Figure 11a, b, c](#) and [d](#)) into an integrated ensemble model ([Figure 12d](#)), supported by the PROMETHEE-GAIA decision-support tool. Our ensemble model combines TOPSIS, VIKOR, EDAS and PROMETHEE-II, with additional insights from PROMETHEE-GAIA. The model builds on recent MCDM applications in the eastern Himalayan floodplains. In the Brahmaputra basin, (Debnath et al. [2023](#)) showed that TOPSIS was among the best-performing single methods ($AUC = 0.920$), followed by VIKOR (0.888) and EDAS (0.746), while machine learning ensembles performed slightly better ($AUC \approx 0.94\text{--}0.95$) (Debnath et al. [2023](#)). They also reported that the estimated area under ‘high’ to ‘very high’ flood susceptibility varied widely with the method used, ranging from about 77,000 to 150,000 km², depending on the threshold rule applied (Debnath et al. [2023](#)). In the Sub-Himalayan foothills of Koch Behar, few scholars tested the results of TOPSIS, VIKOR and EDAS (Mitra and Das [2023](#)). They found good to acceptable performance (all $ROC-AUC > 0.70$), with river islands (chars) and riparian belts consistently identified as the most flood-prone areas (Mitra and Das [2023](#)). A study of Kashmir valley reached similar conclusions, showing that all three models pointed to the Jhelum corridor as highly susceptible, though the share of ‘very high’ zones differed—about 4.3% with TOPSIS, 9.7% with VIKOR, and 5.4% with EDAS (Shah and Pan [2024](#)). These studies show that while MCDM techniques work well across diverse Himalayan regions, results often differ by method. We tried to reinforce the value of hybrid approaches that reduce this uncertainty (Debnath et al. [2023](#); Mitra and Das [2023](#); Shah and Pan [2024](#)). Recent studies show that PROMETHEE performs very well in flood-related applications. In the Spercheios basin, a study reported an AUC of about 0.972, with PROMETHEE even outperforming AHP and TOPSIS, confirming its strength as a key tool in ensemble models (Plataridis and Mallios [2024](#)). Closer to our study area, a Kaljani basin study in Cooch Behar (Koch Bihar) used an AHP–PROMETHEE II hybrid and achieved strong classification results ($F1 \approx 0.88$). However, like most earlier Koch Behar work, that study presented only static maps and summary indices. Our framework goes further by applying PROMETHEE-GAIA, which makes the results more transparent by showing how each criterion influences flood susceptibility and how alternatives compare.

In fact, the hybrid model’s Receiver Operating Characteristic AUC is 0.80, a level generally considered acceptable discrimination for flood susceptibility maps. In contrast, in prior studies no single MCDM model had reached that threshold in Koch Bihar for example, the standalone TOPSIS, VIKOR or EDAS models by seminal works. The hybrid’s superior AUC indicates it was better at correctly identifying both flood-prone and flood-safe areas, reducing false classifications. Moreover, the hybrid framework yielded the lowest Brier Score among models, meaning its probability estimates of flooding were the most well-calibrated to reality (smaller Brier Score denotes less forecast error). Spatial statistics derived from the overlay analysis reinforce these observations. Overall, the Hybrid model classifies about 81% of Koch Bihar’s area as either High or Very High flood susceptibility (with ~43% Very High alone), leaving under 20% as Moderate or lower risk ([Table 5](#)). Within that high-risk expanse, the distribution across blocks is uneven. The block-level analysis showed that 4–5 blocks account for a disproportionate share of the district’s total high-susceptibility area. For example, just the two Tufanganj blocks together contain roughly one-quarter of all the Very High-risk pixels in the district (owing to their large size and floodplain location). Mathabhanga I and the Coch Behar Sadar blocks (I & II) contribute another sizable fraction. In contrast, Sitalkuchi and Sitai each contribute only a small percentage of the total high-risk area. This can be expressed as a percentage of each block affected, as we detailed earlier. Tufanganj II stands out with ~85% of its area under significant flood susceptibility zone (the highest of any block), whereas Sitalkuchi has around 50% (the lowest among major blocks). Most other blocks fall in the 60–80% range, reflecting the pervasive flood exposure in this region.

In terms of proximity to rivers, analysis of spatial statistics confirms that flood-susceptible areas are tightly linked to river geography ([Table 6](#)). District-wise, a large portion (approximately 40%) of all very highly susceptible land lies in immediate riparian zones (within the active channels and adjacent lowlands of major rivers). When measuring distances, we found that over 70% of the High to Very High susceptibility pixels are within 2 km of a major river and over 50% are within just 1 km of a river. Many of the most severe hotspots are essentially right along the riverbanks or on riverine islands (chars).

Table 5. Historical flood frequency, maximum flood depth and hybrid model ratings for different sites in Cooch Behar District.

Site	Block	Influencing Rivers	Historical Flood Frequency	Historical Max Flood Depth (m)	Hybrid Model Rating
Ghughumari	Cooch Behar-I	Torsa	Very High	3.5	Very High
Balabhat	Tufanganj-I	Raidak	Very High	4.2	Very High
Najirhat & Andaranfulbari	Tufanganj-II	Raidak, Kaljani	Very High	4	Very High
Dinhata Municipality	Dinhata-II	Torsa, Dharla	Very High	3.8	Very High
Gitaldaha	Dinhata-I	Dharla	Very High	3.6	Very High
Bhetaguri & Ghoksadanga	Mathabhanga-I & II	Jaldhaka, Mansai	High	3.2	High
Balarampur & Patchhara	Cooch Behar-II	Kaljani, Torsa	High	3	High
Kedarhat	Sitai	Local rivers	High	2.8	Moderate to High
Chamta & Panisala	Mathabhanga-I	Jaldhaka	Moderate	2.5	Moderate
Nakkatigachh & Sahebganj	Dinhata-II	Torsa, Dharla	Moderate	2.2	Moderate
Sitalkuchi	Sitalkuchi	Sutunga & Local streams	Moderate	2	Moderate
Bakshirhat	Tufanganj-II	Raidak	Moderate	2.4	Moderate
Mekhliganj Town	Mekhliganj	Teesta	Low	1.5	Low to Moderate
Haldibari	Haldibari	Localized Rainfall	Rare	1	Low

Source: Calculated by the authors.

Table 6. Block-wise historical flood frequency, hybrid model susceptibility and flood-prone area analysis in Cooch Behar District.

Block	Historical Flood Frequency (Avg. Score)	Hybrid Model Susceptibility (Avg. Score)	Major Influencing Rivers	Avg. Flood Depth (m)	Flood Prone Area (%)	Avg. Distance to Nearest River (km)
Cooch Behar-I	4.8	4.7	Torsa	3.8	78	1.2
Cooch Behar-II	4.5	4.6	Kaljani, Torsa	3.5	72	1.5
Dinhata-I	5	5	Torsa, Dharla	4.2	85	0.8
Dinhata-II	4.2	4.3	Torsa, Dharla	3.9	75	1
Mathabhanga-I	4.6	4.5	Jaldhaka	3.7	79	1.3
Mathabhanga-II	4.3	4.2	Jaldhaka	3.6	76	1.4
Tufanganj-I	5	5	Raidak	4.5	88	0.6
Tufanganj-II	5	5	Raidak, Kaljani	4.8	90	0.5
Sitalkuchi	3.2	3.5	Sutunga	2.7	55	2.2
Sitai	3	3	Local Streams	2.5	50	2.5
Mekhliganj	2.5	2.8	Teesta	1.9	40	3
Haldibari	1.5	1.8	Localized Rainfall	1.2	25	4

Source: Calculated by the authors.

For instance, the average distance of Very High susceptibility areas in Tufanganj I and II from the nearest river is only ~0.8 km, highlighting that these zones hug the Raidak River closely. Even in blocks like Cooch Behar I and II, the city's flood susceptibility zones correspond to the Torsa and Kaljani riverbeds that run through or near the town. Despite the broad agreement in which areas are at risk, the models do show some differences in the extent and intensity of predicted risk. Notably, TOP_PROM (Figure 12a) and VIKOR_PROM tended to classify a slightly larger portion of the district as 'Very High' risk, while ED_PROM (Figure 12c) was somewhat more conservative. Specifically, TOPSIS-PROMETHEE and VIKOR-PROMETHEE (Figure 12b) each marked about 42–43% of the total area as Very High

susceptibility, whereas the EDAS-PROMETHEE model marked around 39.8%. These differences imply that the TOPSIS and VIKOR combined models may overestimate extreme risk zones slightly (painting more area in the highest risk class), while EDAS combined model slightly underestimates them by keeping more area in High or Moderate classes. The hybrid model falls in between: it identified roughly 43.2% of the area as Very High susceptibility, comparable to TOPSIS-VIKOR, but it also adjusted (reduced or redistributed) the High vs Very High extents by about 5–8% to avoid over-prediction. In practice, this means the Hybrid map might label some fringe areas as ‘High’ instead of ‘Very High’, smoothing out the extremities that TOPSIS_PROM and VIKOR_PROM showed. Conversely, the Hybrid model expanded a few High-risk areas that ED_PROM might have only marked moderate, ensuring critical zones are not missed.

Official flood reports and local studies highlight both natural and anthropogenic causes for Koch Bihar’s chronic flooding. Intense monsoon rainfall (often exceeding 250–300 mm in 24 hours) in the upstream catchments causes rivers to swell rapidly, leading to sudden inundation downstream. Preliminary validation suggests the Hybrid model achieves noticeably better accuracy in forecasting inundation extent. For instance, its simulated flood zones for recent events overlap ~90% of observed flooded areas, versus ~75–80% overlap for prior models. This boost in accuracy means fewer missed flood-prone spots and reduced false alarms. Historical flood footprints derived from Sentinel-1 SAR data (Figure 16a & d, representing the 2017 flood event) closely match the outputs from the Hybrid model of Flood Susceptibility Mapping (FSM) (Figure 16c & f). This strong correlation indicates robust reliability and accuracy of the hybrid approach. Moreover, global river flood hazard maps generated from the LISFLOOD hydrodynamic model (Figure 16b & e) further validate the hybrid outputs by demonstrating consistent flood-prone areas.

Unlike earlier susceptibility maps, which categorized risk primarily at single MCDM model, the Hybrid model provides significantly more granular flood predictions within each block. A key feature of the Hybrid model is its iterative calibration and validation against actual flood events. Specifically, the 2017 flood event, analysed using Sentinel-1 dual-polarization C-band SAR data (Ground Range Detected, GRD scenes with VV + VH polarization at resolutions of 10 to 40 meters), has been utilized to fine-tune model parameters, significantly improving predictive accuracy and enhancing confidence in identifying high-risk zones. By incorporating real-time rainfall data and upstream flow inputs, the model offers superior prediction capability for flash floods with improved lead time, marking a substantial advancement over previous susceptibility maps, including those based on AHP methodology, which identified broad risk zones but were not event-specific.

7. Conclusion

This study delivers a high-resolution, decision-ready flood susceptibility assessment for Cooch Behar (Koch Bihar) by hybridizing TOPSIS, VIKOR, EDAS and PROMETHEE-II and interpreting results with PROMETHEE-GAIA. The ensemble improves on single-method baselines by combining higher predictive skill, greater rank stability and transparent criterion insights. Susceptibility peaks consistently along the Torsa, Raidak, Jaldhaka and Kaljani corridors, with Tufanganj I & II, Mathabhanga I and Cooch Behar I & II emerging as priority blocks patterns that align with known riparian and char-island exposures. These outputs convert complex multi-factor evidence into actionable zoning for preparedness and mitigation. Validation shows strong discriminatory power ($\text{ROC-AUC} > 0.75$) and better calibration (lowest Brier Score among tested models), while sensitivity tests indicate that top-decile hotspots remain stable to plausible weight perturbations. Beyond accuracy, Promethee-GAIA plots surface why locations rank highly exposing criterion vectors (e.g. slope/TRI vs. TWI/MNDWI) and clarifying trade-offs thereby improving trust and uptake by planners. Practically, the maps and block wise summaries support targeted interventions within 1–2 km of major channels, prioritizing embankment strengthening, drainage management and land-use regulation. Our modelling estimates susceptibility (physical likelihood) rather than full risk (which also requires exposure and vulnerability). Although our framework is a susceptibility tool, it directly improves flood mitigation by sharpening resource targeting and pinpointing priority blocks (e.g. Tufanganj I & II, Mathabhanga I, Koch Bihar I & II) and 1–2 km river corridors for pre-positioning materials, embankment maintenance and evacuation route planning. Compared with single-method

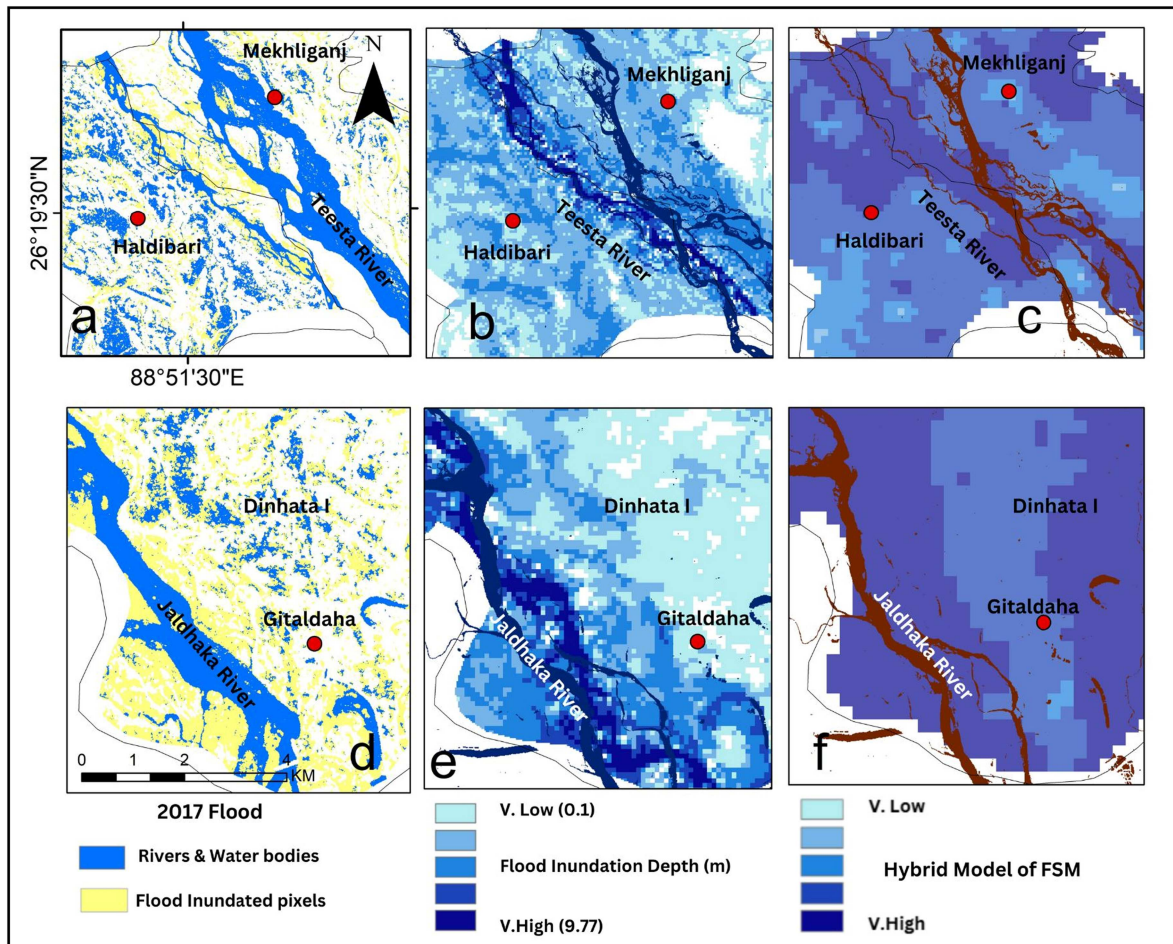


Figure 16. Comparative flood susceptibility and inundation mapping for Koch Bihar District: (a) 2017 Flood Inundation from Sentinel-1 SAR Data (Mekhliganj–Haldibari), (b) Global River Flood Hazard Maps (GRFHM), (c) Hybrid Model of Flood Susceptibility Mapping (FSM), (d) 2017 flood inundation from Sentinel-1 SAR Data (Gitaldaha of Dinhata-I block), (e) Global River Flood Hazard Maps (Gitaldaha of Dinhata-I block) and (f) Hybrid Model of Flood Susceptibility Mapping (FSM).

zoning, the hybrid provides higher discrimination and better calibration. The PROMETHEE-GAIA makes the ‘why’ behind high-ranked zones transparent, which builds stakeholder trust and speeds inter-departmental buy-in. If we link the model to routine rainfall and river-stage feeds or hydrodynamic models, these layers can act as a triage surface for early-warning dashboards. If we touch upon the basic limitations of this model, the socio-economic layers were not integrated. The calibration process relies on a small set of past flood events, so estimates may shift under different settings. Further work can be done moving from susceptibility to full risk by adding exposure and vulnerability layers (population, infrastructure, critical facilities). At the planning level, outputs can inform urban growth regulation, embankment strengthening, drainage network design and land-use zoning, especially in flood-prone corridors such as Tufanganj, Mathabhanga, and Cooch Behar blocks. Because the workflow is GIS-based, reproducible and relatively low-cost, it can be embedded into state disaster management systems or shared across India-Bangladesh transboundary flood coordination platforms.

Acknowledgements

The authors sincerely acknowledge the Copernicus Open Access Hub (ESA) for providing Sentinel-1 SAR data, the European Soil Data Centre (ESDAC) - European Commission, and the European Commission, Joint Research Centre (JRC) for valuable geospatial datasets. We are also grateful to ESRI for GIS resources and IMD Pune (imdpune.gov.in) for meteorological data. Special thanks to the District Magistrate of Cooch Behar (Koch Bihar), the Disaster Management Cell of the district, and the local residents for their insights and ground validation support.

Author contributions

CRedit: **Debarshi Ghosh:** Conceptualization, Data curation, Formal analysis, Methodology, Resources, Supervision, Validation, Visualization, Writing – original draft, Writing – review & editing; **Sanjoy Mandal:** Methodology, Validation; **Dipankar Das:** Conceptualization, Data curation, Formal analysis, Methodology, Resources, Software, Validation, Writing – review & editing; **Edris Alam:** Funding acquisition, Methodology, Validation; **Snehasish Saha:** Formal analysis, Investigation, Methodology, Supervision, Writing – original draft, Writing – review & editing.

Disclosure statement

The authors declare no competing interests.

ORCID

Debarshi Ghosh  0000-0001-9673-5762

Sanjoy Mandal  0009-0003-6135-1525

Dipankar Das  0000-0003-0266-9990

Edris Alam  0000-0001-7303-9625

Data availability statement

Data generated for this study can be obtained from the first author upon reasonable request.

References

- Abdel Hamid HT, Wenlong W, Qiaomin L. 2020. Environmental sensitivity of flash flood hazard using geospatial techniques. *Glob J Environ Sci Manag.* 6(1):31–46. <https://doi.org/10.22034/GJESM.2020.01.03>
- Abdullah MF, Siraj S, Hodgett RE. 2021. An overview of multi criteria decision analysis (MCDA) application in managing water-related disaster events. *Water (Switzerland).* 13(10):1358. <https://doi.org/10.3390/w13101358>
- Abedi Gheshlaghi H, Feizizadeh B, Blaschke T. 2020. GIS-based forest fire risk mapping using the analytical network process and fuzzy logic. *J Environ Plann Manage.* 63(3):481–499. <https://doi.org/10.1080/09640568.2019.1594726>
- Acharya B, Joshi B. 2020. Flood frequency analysis for an ungauged himalayan river basin using different methods: a case study of modi khola, parbat, Nepal. *Meteorol Hydrol Water Manag.* 8(2):46–51. <https://doi.org/10.26491/mhwm/131092>
- Ahmad Z et al. 2019. Mitigation of toxic effects caused by tartrazine in wistar rats through oral administration of melon seed oil. *Pak J Agric Sci.* 56(2):435–442. <https://doi.org/10.21162/PAKJAS/19.6782>
- Akay H. 2021. Flood hazards susceptibility mapping using statistical, fuzzy logic, and MCDM methods. *Soft Computing.* 25(14):9325–9346. <https://doi.org/10.1007/S00500-021-05903-1>
- AlAli AM, Salih A, Hassaballa A. 2023. Geospatial-based analytical hierarchy process (AHP) and weighted product model (WPM) techniques for mapping and assessing flood susceptibility in the wadi hanifah drainage basin, Riyadh region, Saudi Arabia. *Water (Switzerland).* 15(10):1943. <https://doi.org/10.3390/W15101943>
- Al-Areeq AM, Saleh RAA, Ghaleb M, Abba SI, Yaseen ZM. 2024. Implication of novel hybrid machine learning model for flood subsidence susceptibility mapping: a representative case study in Saudi Arabia. *J Hydrol.* 630:130692. <https://doi.org/10.1016/j.jhydrol.2024.130692>
- Al-Areeq AM, Abba SI, Yassin MA, Benaaf M, Ghaleb M, Aljundi IH. 2022. Computational machine learning approach for flood susceptibility assessment integrated with remote sensing and GIS techniques from jeddah, Saudi Arabia. *Remote Sens.* 14(21):5515. <https://doi.org/10.3390/RS14215515>
- Alarifi SS, Abdelkareem M, Abdalla F, Alotaibi M. 2022. Flash flood hazard mapping using remote sensing and GIS techniques in southwestern Saudi Arabia. *Sustainability (Switzerland).* 14(21):14145. <https://doi.org/10.3390/SU142114145>
- Arabameri A, Pradhan B, Pourghasemi HR, Rezaei K. 2018. Identification of erosion-prone areas using different multi-criteria decision-making techniques and gis. *Geomat Natural Hazards Risk.* 9(1):1129–1155. <https://doi.org/10.1080/19475705.2018.1513084>
- Aruchsamay R, Velusamy I, Sanmugavel K, Dhandapani PB, Ramasamy K. 2024. Generalization of fermatean fuzzy set and implementation of fermatean fuzzy PROMETHEE II method for decision making via PROMETHEE GAIA. *Axioms.* 13(6):408. <https://doi.org/10.3390/axioms13060408>
- Ashfaq S, Tufail M, Niaz A, Muhammad S, Alzahrani H, Tariq A. 2025. Flood susceptibility assessment and mapping using GIS-based analytical hierarchy process and frequency ratio models. *GPC.* 251:104831. <https://doi.org/10.1016/J.GLOPLACHA.2025.104831>
- Avand M, Moradi H, lasboyee MR. 2021. Using machine learning models, remote sensing, and GIS to investigate the effects of changing climates and land uses on flood probability. *J Hydrol.* 595:125663. <https://doi.org/10.1016/j.jhydrol.2020.125663>
- Bannari A, El-Battay A, Hameid N, Tashtoush F. 2017. Salt-affected soil mapping in an arid environment using semi-empirical model and Landsat-OLI data. *Adv Remote Sens.* 06(04):260–291. <https://doi.org/10.4236/ars.2017.64019>

- Barros JL, Tavares AO, Santos PP, Freire P. **2022**. Enhancing a coastal territorial vulnerability index: anticipating the impacts of coastal flooding with a local scale approach. *Coastal Management*. 50(5):442–468. <https://doi.org/10.1080/08920753.2022.2107858>
- Behzadian M, Kazemzadeh RB, Albadvi A, Aghdasi M. **2010**. PROMETHEE: a comprehensive literature review on methodologies and applications. *Eur J Oper Res*. 200(1):198–215. <https://doi.org/10.1016/j.ejor.2009.01.021>
- de Brito MM, Almoradie A, Evers M. **2019**. Spatially-explicit sensitivity and uncertainty analysis in a MCDA-based flood vulnerability model. *Int J Geogr Inf Sci*. 33(9):1788–1806. <https://doi.org/10.1080/13658816.2019.1599125>
- de Brito MM, Evers M. **2016**. Multi-criteria decision-making for flood risk management: a survey of the current state of the art. *Nat Hazards Earth Syst Sci*. 16:1019–1033. <https://doi.org/10.5194/nhess-16-1019-2016>
- Bui DT et al. **2019**. A novel hybrid approach based on a swarm intelligence optimized extreme learning machine for flash flood susceptibility mapping. *Catena*. 179(October 2018):184–196. <https://doi.org/10.1016/j.catena.2019.04.009>
- Bui QT, Nguyen QH, Nguyen XL, Pham VD, Nguyen HD, Pham VM. **2020**. Verification of novel integrations of swarm intelligence algorithms into deep learning neural network for flood susceptibility mapping. *J Hydrol*. 581:124379. <https://doi.org/10.1016/j.jhydrol.2019.124379>
- Carrington AM et al. **2023**. Deep ROC analysis and AUC as balanced average accuracy, for improved classifier selection, audit and explanation. *ITPAM*. 45(1):329–341. <https://doi.org/10.1109/TPAMI.2022.3145392>
- Castelló-Sirvent F, Meneses-Eraso C, Alonso-Gómez J, Peris-Ortiz M. **2022**. Three decades of fuzzy AHP: a bibliometric analysis. *Axioms*. 11(10):525. <https://doi.org/10.3390/axioms11100525>
- Chakraborty S, Mukhopadhyay S. **2019**. Assessing flood risk using analytical hierarchy process (AHP) and geographical information system (GIS): application in coochbehar district of west bengal, India. *Nat Hazards*. 99(1):247–274. <https://doi.org/10.1007/s11069-019-03737-7>
- Chapi K et al. **2017**. A novel hybrid artificial intelligence approach for flood susceptibility assessment. *Environ Modell Softw*. 95:229–245. <https://doi.org/10.1016/j.envsoft.2017.06.012>
- Choudhury S, Basak A, Biswas S, Das J. **2022**. Flash flood susceptibility mapping using GIS-based AHP method. In: Pradhan B, Shit PK, Bhunia GS, Adhikary PP, Pourghasemi HR, editors. *Spatial modelling of flood risk and flood hazards: Societal implications*. Springer. p 119–142. https://doi.org/10.1007/978-3-030-94544-2_8
- Debnath J et al. **2023**. Evaluating Flood Susceptibility in the Brahmaputra River Basin: An Insight into Asia's Eastern Himalayan Floodplains Using Machine Learning and Multi-Criteria Decision-Making. *Earth Syst Environ*. 7:733–760. <https://doi.org/10.1007/s41748-023-00358-w>
- Demissie Z, Rimal P, Seyoum WM, Dutta A, Rimmington G. **2024**. Flood susceptibility mapping: integrating machine learning and GIS for enhanced risk assessment. *Appl Comput Geosci*. 23:100183. <https://doi.org/10.1016/J.ACAGS.2024.100183>
- Dormann CF et al. **2013**. Collinearity: a review of methods to deal with it and a simulation study evaluating their performance. *Ecography*. 36(1):27–46. <https://doi.org/10.1111/j.1600-0587.2012.07348.x>
- Duchemin M, Hogue R. **2009**. Reduction in agricultural non-point source pollution in the first year following establishment of an integrated grass/tree filter strip system in Southern quebec (Canada). *Agric Ecosyst Environ*. 131(1–2):85–97. <https://doi.org/10.1016/j.agee.2008.10.005>
- Fawcett T. **2006**. An introduction to ROC analysis. *Pattern Recognit Lett*. 27(8):861–874. <https://doi.org/10.1016/j.patrec.2005.10.010>
- Ghobadi M, Ahmadipari M. **2024**. Enhancing flood susceptibility modeling: a hybrid deep neural network with statistical learning algorithms for predicting flood prone areas. *Water Resour Manage*. 38(8):2687–2710. <https://doi.org/10.1007/s11269-024-03770-7>
- Ghorbani MA, Jabehdar MA, Yaseen ZM, Inyurt S. **2021**. Solving the pan evaporation process complexity using the development of multiple mode of neurocomputing models. *Theor Appl Climatol*. 145(3–4):1521–1539. <https://doi.org/10.1007/s00704-021-03724-8>
- Ghorbanzadeh O, Didehbani K, Rasouli H, Kamran KV, Feizizadeh B, Blaschke T. **2020**. An application of sentinel-1, sentinel-2, and GNSS data for landslide susceptibility mapping. *IJGI*. 9(10):561. <https://doi.org/10.3390/ijgi9100561>
- Ghosh M, Ghosal S. **2021**. Climate change vulnerability of rural households in flood-prone areas of himalayan foothills, west bengal, India. *Environ Dev Sustain*. 23(2):2570–2595. <https://doi.org/10.1007/s10668-020-00687-0>
- Ghosh S, Saha S, Bera B. **2022**. Flood susceptibility zonation using advanced ensemble machine learning models within himalayan foreland basin. *Nat Hazards Res*. 2(4):363–374. <https://doi.org/10.1016/j.nhres.2022.06.003>
- Islam R. **2025**. Chapter 17 Addressing Food Security in Bangladesh Associated with Climate Change. February.
- Kar S et al. **2022**. A model-based prediction and analysis of seasonal and tidal influence on pollutants distribution from city outfalls of river Ganges in west bengal, India and its mapping using GIS tool. *PLOS Water*. 1(2):e0000008. <https://doi.org/10.1371/journal.pwat.0000008>
- Kazakis N, Koulias I, Patsialis T. **2015**. Assessment of flood hazard areas at a regional scale using an index-based approach and analytical hierarchy process: application in Rhodope-evros region, Greece. *Sci Total Environ*. 538:555–563. <https://doi.org/10.1016/j.scitotenv.2015.08.055>
- Khosravi K et al. **2018**. A comparative assessment of decision trees algorithms for flash flood susceptibility modeling at haraz watershed, Northern Iran. *Sci Total Environ*. 627:744–755. <https://doi.org/10.1016/j.scitotenv.2018.01.266>
- Khosravi K et al. **2020**. Convolutional neural network approach for spatial prediction of flood hazard at national scale of Iran. *J Hydrol*. 591:125552. <https://doi.org/10.1016/j.jhydrol.2020.125552>

- Kumar R, Acharya P. 2016. Flood hazard and risk assessment of 2014 floods in kashmir valley: a space-based multisensor approach. *Nat Hazards*. 84(1):437–464. <https://doi.org/10.1007/s11069-016-2428-4>
- Kyriazos T, Poga M. 2023. Dealing with multicollinearity in factor analysis: the problem, detections, and solutions. *Open J Statistics*. 13(03):404–424. <https://doi.org/10.4236/ojs.2023.133020>
- Liu L et al. 2015. Developing an effective 2-D urban flood inundation model for city emergency management based on cellular automata. *NHESS*. 15(3):381–391. <https://doi.org/10.5194/nhess-15-381-2015>
- Lorch RF, Myers JL. 1990. Regression analyses of repeated measures data in cognitive research. *J Exp Psychol: Learn Mem Cogn*. 16(1):149–157. <https://doi.org/10.1037/0278-7393.16.1.149>
- Lyu HM, Wang GF, Shen JS, Lu LH, Wang GQ. 2016. Analysis and GIS mapping of flooding hazards on 10 May 2016, guangzhou, China. *Water (Switzerland)*. 8(10):1–17. <https://doi.org/10.3390/w8100447>
- Malczewski J. 1999. *GIS and Multicriteria Decision Analysis*. John Wiley & Sons.
- Mandrekar JN. 2010. Receiver operating characteristic curve in diagnostic test assessment. *J Thorac Oncol*. 5(9):1315–1316. <https://doi.org/10.1097/JTO.0B013E3181EC173D>
- Maqsoom A et al. 2021. Efficiency of multiple hybrid techniques for the earthquake physical susceptibility mapping: the case of abbottabad district, Pakistan. *EES*. 80(19):1–20. <https://doi.org/10.1007/s12665-021-09964-1>
- Menard C, Duncan P, Fleurance G, Georges JY, Lila M. 2002. Comparative foraging and nutrition of horses and cattle in european wetlands. *J Appl Ecol*. 39(1):120–133. <https://doi.org/10.1046/j.1365-2664.2002.00693.x>
- Midi H, Bagheri A. 2010. Robust multicollinearity diagnostic measure in collinear data set. In: *International Conference on Applied Mathematics, Simulation, Modelling - Proceedings*. p 138–142.
- Mitra R, Das J. 2023. A comparative assessment of flood susceptibility modelling of GIS-based TOPSIS, VIKOR, and EDAS techniques in the Sub-Himalayan foothills region of Eastern India. *Environ Sci Pollut Res*. 30:16036–16067. <https://doi.org/10.1007/s11356-022-23168-5>
- Mitra R, Saha P, Das J. 2022. Assessment of the performance of GIS-based analytical hierarchical process (AHP) approach for flood modelling in uttar dinajpur district of west bengal, India. *Geomat Nat Hazards Risk*. 13(1):2183–2226. <https://doi.org/10.1080/19475705.2022.2112094>
- Mosavi A, Ozturk P, Chau KW. 2018. Flood prediction using machine learning models: literature review. *Water (Switzerland)*. 10(11):1–40. <https://doi.org/10.3390/w10111536>
- Nguyen HM, Bae DH. 2019. An approach for improving the capability of a coupled meteorological and hydrological model for rainfall and flood forecasts. *J Hydrol*. 577:124014. <https://doi.org/10.1016/j.jhydrol.2019.124014>
- O'Brien RM. 2007. A caution regarding rules of thumb for variance inflation factors. *Qual Quant*. 41(5):673–690. <https://doi.org/10.1007/s11135-006-9018-6>
- Ouma YO, Tateishi R. 2014. Urban flood vulnerability and risk mapping using integrated multi-parametric AHP and GIS: methodological overview and case study assessment. *Water (Switzerland)*. 6(6):1515–1545. <https://doi.org/10.3390/w6061515>
- Pai SY et al. 2014. Flow cytometry diagnosis of dedicator of cytokinesis 8 (DOCK8) deficiency. *J Allergy Clin Immunol*. 134(1):221–223.e7. <https://doi.org/10.1016/j.jaci.2014.02.023>
- Panahi M et al. 2021. Deep learning neural networks for spatially explicit prediction of flash flood probability. *Geosci Front*. 12(3):101076. <https://doi.org/10.1016/j.gsf.2020.09.007>
- Paul GC, Saha S, Hembram TK. 2019. Application of the GIS-Based probabilistic models for mapping the flood susceptibility in bansloi sub-basin of ganga-bhagirathi river and their comparison. *RSESS*. 2(2–3):120–146. <https://doi.org/10.1007/s41976-019-00018-6>
- Plataridis K, Mallios Z. 2024. Mapping flood susceptibility with PROMETHEE multi-criteria analysis method. *Environ Sci Pollut Res*. 31:41267–41289. <https://doi.org/10.1007/s11356-024-33895-6>
- Pham BT et al. 2021. Flood risk assessment using deep learning integrated with multi-criteria decision analysis. *Knowl-Based Syst*. 219:106899. <https://doi.org/10.1016/j.knosys.2021.106899>
- Pourghasemi HR et al. 2020. Assessing and mapping multi-hazard risk susceptibility using a machine learning technique. *NatSR*. 10(1):1–11. <https://doi.org/10.1038/s41598-020-60191-3>
- Rahmati O et al. 2020. Development of novel hybridized models for urban flood susceptibility mapping. *NatSR*. 10(1):1–19. <https://doi.org/10.1038/s41598-020-69703-7>
- Rana MS, Mahanta C. 2023. Spatial prediction of flash flood susceptible areas using novel ensemble of bivariate statistics and machine learning techniques for ungauged region. *Nat Hazards*. 115(1):947–969. <https://doi.org/10.1007/s11069-022-05580-9>
- Razavi Termeh SV, Kornejady A, Pourghasemi HR, Keesstra S. 2018. Flood susceptibility mapping using novel ensembles of adaptive neuro fuzzy inference system and metaheuristic algorithms. *Sci Total Environ*. 615:438–451. <https://doi.org/10.1016/j.scitotenv.2017.09.262>
- Roy S, Bose A, Chowdhury IR. 2021. Flood risk assessment using geospatial data and multi-criteria decision approach: a study from historically active flood-prone region of himalayan foothill, India. *Arabian J Geosci*. 14(11):999. <https://doi.org/10.1007/s12517-021-07324-8>
- Shah AI, Pan ND. 2024. Flood susceptibility assessment of Jhelum River Basin: A comparative study of TOPSIS, VIKOR and EDAS methods. *Geosystems and Geoenvironment*. 3(4):100304<https://doi.org/10.1016/j.geogeo.2024.100304>
- Saha UD, Alam MJ, Bhattacharya S, Majumder A. 2023. Nature of flood and channel sedimentation in the torsa river: a hydro-geomorphic study. In: *Springer Geography*. June. p 37–61. https://doi.org/10.1007/978-3-031-21086-0_3

- Samanta RK, Bhunia GS, Shit PK, Pourghasemi HR. 2018. Flood susceptibility mapping using geospatial frequency ratio technique: a case study of Subarnarekha River Basin, India. *Model Earth Syst Environ.* 4:395–408. <https://doi.org/10.1007/s40808-018-0427-z>
- Shams H, Khan A, Haleem K, Mahmood S. 2024. Assessing the effects of climate and land-use change on flood recurrence in kokcha river, Afghanistan. *J Water Clim Change.* 15(5):2464–2483. <https://doi.org/10.2166/wcc.2024.043>
- Srivastava PK, Bhattacharya AK. 2006. Groundwater assessment through an integrated approach using remote sensing, GIS and resistivity techniques: a case study from a hard rock terrain. *Int J Remote Sens.* 27(20):4599–4620. <https://doi.org/10.1080/01431160600554983>
- Tehrany MS, Kumar L, Shabani F. 2019. A novel GIS-based ensemble technique for flood susceptibility mapping using evidential belief function and support vector machine: Brisbane, Australia. *PeerJ.* 2019(10):e7653. <https://doi.org/10.7717/peerj.7653>
- Yariyan P et al. 2020. Flood susceptibility mapping using an improved analytic network process with statistical models. *Geomat Nat Hazards Risk.* 11(1):2282–2314. <https://doi.org/10.1080/19475705.2020.1836036>
- Zhao G et al. 2021. Improving urban flood susceptibility mapping using transfer learning. *J Hydrol.* 602(August):126777. <https://doi.org/10.1016/j.jhydrol.2021.126777>
- Zorlu K, Dede V. 2023. Evaluation of nature-based tourism potential in protected and sensitive areas by CRITIC and PROMETHEE-GAIA methods. *Int J Geoheritage Parks.* 11(3):349–364. <https://doi.org/10.1016/j.ijgeop.2023.05.004>
- Zuur AF, Ieno EN, Elphick CS. 2010. A protocol for data exploration to avoid common statistical problems. *Methods Ecol Evol.* 1(1):3–14. <https://doi.org/10.1111/j.2041-210x.2009.00001.x>